IEC 61788-17

Edition 2.0 2021-04
REDLINE VERSION

INTERNATIONAL STANDARD

colour inside

Superconductivity –
Part 17: Electronic characteristic measurements – Local critical current density and its distribution in large-area superconducting films

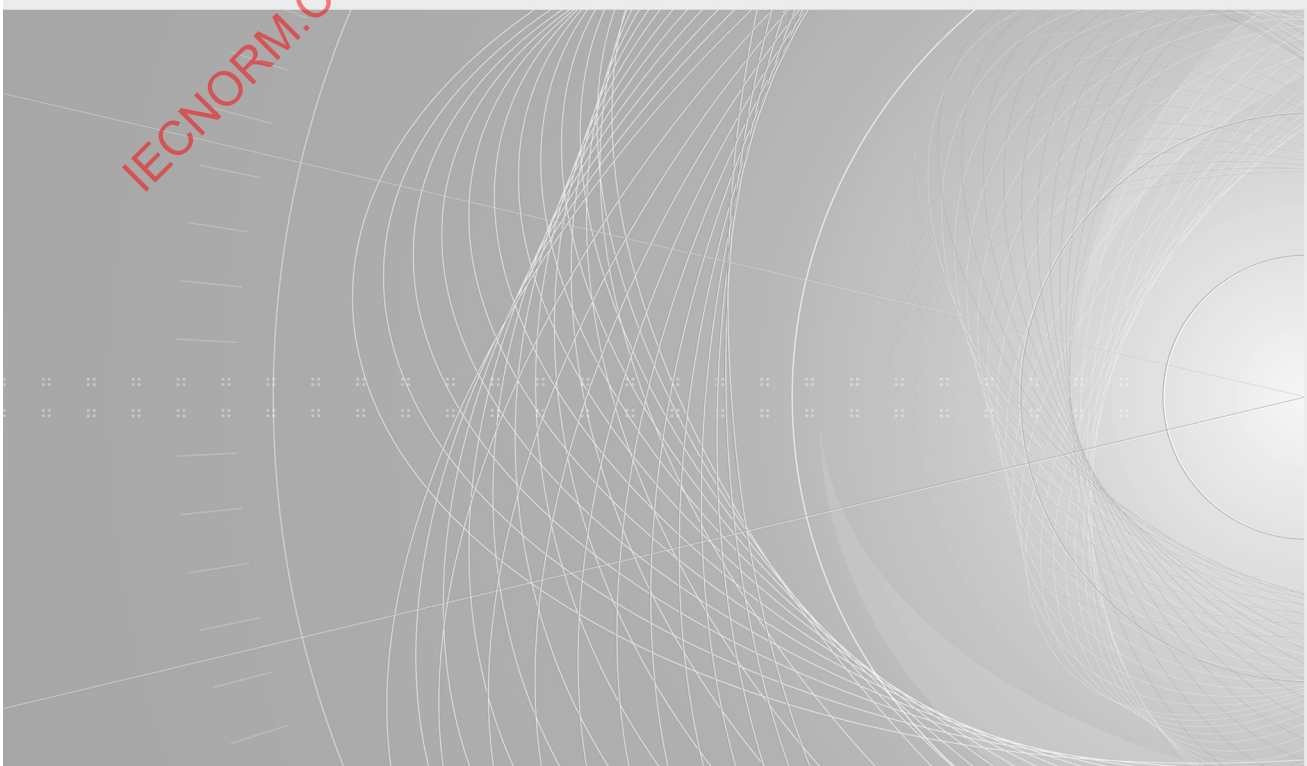

IEC 61788-17:2021-04 RLV(en)

IEC Central Office
3, rue de Varembé
CH-1211 Geneva 20
Switzerland

Tel.: +41 22 919 02 11
info@iec.ch
www.iec.ch

About the IEC
The International Electrotechnical Commission (IEC) is the leading global organization that prepares and publishes International Standards for all electrical, electronic and related technologies.

About IEC publications
The technical content of IEC publications is kept under constant review by the IEC. Please make sure that you have the latest edition, a corrigendum or an amendment might have been published.

IEC publications search - webstore.iec.ch/advsearchform
The advanced search enables to find IEC publications by a variety of criteria (reference number, text, technical committee, …). It also gives information on projects, replaced and withdrawn publications.

IEC Just Published - webstore.iec.ch/justpublished
Stay up to date on all new IEC publications. Just Published details all new publications released. Available online and once a month by email.

IEC Customer Service Centre - webstore.iec.ch/csc
If you wish to give us your feedback on this publication or need further assistance, please contact the Customer Service Centre: sales@iec.ch.

IEC online collection - oc.iec.ch
Discover our powerful search engine and read freely all the publications previews. With a subscription you will always have access to up to date content tailored to your needs.

Electropedia - www.electropedia.org
The world's leading online dictionary on electrotechnology, containing more than 22 000 terminological entries in English and French, with equivalent terms in 18 additional languages. Also known as the International Electrotechnical Vocabulary (IEV) online.

IEC 61788-17

Edition 2.0 2021-04
REDLINE VERSION

INTERNATIONAL STANDARD

colour inside

Superconductivity –
Part 17: Electronic characteristic measurements – Local critical current density and its distribution in large-area superconducting films

INTERNATIONAL
ELECTROTECHNICAL
COMMISSION

ICS 17.220.20; 29.050

ISBN 978-2-8322-9765-0

CONTENTS

INTERNATIONAL ELECTROTECHNICAL COMMISSION

_____

SUPERCONDUCTIVITY –

Part 17: Electronic characteristic measurements – Local critical current density and its distribution in large-area superconducting films

FOREWORD

1) The International Electrotechnical Commission (IEC) is a worldwide organization for standardization comprising all national electrotechnical committees (IEC National Committees). The object of IEC is to promote international co-operation on all questions concerning standardization in the electrical and electronic fields. To this end and in addition to other activities, IEC publishes International Standards, Technical Specifications, Technical Reports, Publicly Available Specifications (PAS) and Guides (hereafter referred to as "IEC Publication(s)"). Their preparation is entrusted to technical committees; any IEC National Committee interested in the subject dealt with may participate in this preparatory work. International, governmental and non-governmental organizations liaising with the IEC also participate in this preparation. IEC collaborates closely with the International Organization for Standardization (ISO) in accordance with conditions determined by agreement between the two organizations.
2) The formal decisions or agreements of IEC on technical matters express, as nearly as possible, an international consensus of opinion on the relevant subjects since each technical committee has representation from all interested IEC National Committees.
3) IEC Publications have the form of recommendations for international use and are accepted by IEC National Committees in that sense. While all reasonable efforts are made to ensure that the technical content of IEC Publications is accurate, IEC cannot be held responsible for the way in which they are used or for any misinterpretation by any end user.
4) In order to promote international uniformity, IEC National Committees undertake to apply IEC Publications transparently to the maximum extent possible in their national and regional publications. Any divergence between any IEC Publication and the corresponding national or regional publication shall be clearly indicated in the latter.
5) IEC itself does not provide any attestation of conformity. Independent certification bodies provide conformity assessment services and, in some areas, access to IEC marks of conformity. IEC is not responsible for any services carried out by independent certification bodies.
6) All users should ensure that they have the latest edition of this publication.
7) No liability shall attach to IEC or its directors, employees, servants or agents including individual experts and members of its technical committees and IEC National Committees for any personal injury, property damage or other damage of any nature whatsoever, whether direct or indirect, or for costs (including legal fees) and expenses arising out of the publication, use of, or reliance upon, this IEC Publication or any other IEC Publications.
8) Attention is drawn to the Normative references cited in this publication. Use of the referenced publications is indispensable for the correct application of this publication.
9) Attention is drawn to the possibility that some of the elements of this IEC Publication may be the subject of patent rights. IEC shall not be held responsible for identifying any or all such patent rights.

This redline version of the official IEC Standard allows the user to identify the changes made to the previous edition IEC 61788-17:2013. A vertical bar appears in the margin wherever a change has been made. Additions are in green text, deletions are in strikethrough red text.

IEC 61788-17 has been prepared by IEC technical committee 90: Superconductivity. It is an International Standard.

This second edition cancels and replaces the first edition published in 2013. This edition constitutes a technical revision.

This edition includes the following a significant technical change with respect to the previous edition:

a) A simple method to calculate theoretical coil coefficient k is described in 6.2.1.

The text of this International Standard is based on the following documents:

FDIS	Report on voting
90/462/FDIS	90/464/RVD

Full information on the voting for the approval of this International Standard can be found in the report on voting indicated in the above table.

The language used for the development of this International Standard is English.

This document was drafted in accordance with ISO/IEC Directives, Part 2, and developed in accordance with ISO/IEC Directives, Part 1 and ISO/IEC Directives, IEC Supplement, available at www.iec.ch/members_experts/refdocs. The main document types developed by IEC are described in greater detail at www.iec.ch/standardsdev/publications.

A list of all the parts of the IEC 61788 series, published under the general title *Superconductivity*, can be found on the IEC website.

The committee has decided that the contents of this document will remain unchanged until the stability date indicated on the IEC website under "http://webstore.iec.ch" in the data related to the specific document. At this date, the document will be

- reconfirmed,
- withdrawn,
- replaced by a revised edition, or
- amended.

IMPORTANT – The 'colour inside' logo on the cover page of this publication indicates that it contains colours which are considered to be useful for the correct understanding of its contents. Users should therefore print this document using a colour printer.

INTRODUCTION

Over thirty years after their discovery in 1986, high-temperature superconductors are now finding their way into products and technologies that will revolutionize information transmission, transportation, and energy. Among them, high-temperature superconducting (HTS) microwave filters, which exploit the extremely low surface resistance of superconductors, have already been commercialized. They have two major advantages over conventional non-superconducting filters, namely: low insertion loss (low noise characteristics) and high frequency selectivity (sharp cut) [1][1]. These advantages enable a reduced number of base stations, improved speech quality, more efficient use of frequency bandwidths, and reduced unnecessary radio wave noise.

Large-area superconducting thin films have been developed for use in microwave devices [2]. They are also ~~used~~ considered for use in emerging superconducting power devices, such as resistive-type superconducting fault-current limiters (SFCLs) [3] [4] [5], superconducting fault detectors used for superconductor-triggered fault current limiters [6] [7] and persistent-current switches used for persistent-current HTS magnets [8] [9]. The critical current density J_c is one of the key parameters that describe the quality of large-area HTS films. Nondestructive, AC inductive methods are widely used to measure J_c and its distribution for large-area HTS films [10] [11] [12] [13], among which the method utilizing third-harmonic voltages $U_3\cos(3\omega t + \theta)$ is the most popular [10] [11], where ω, t and θ denote the angular frequency, time, and initial phase, respectively. However, these conventional methods are not accurate because they have not considered the electric-field E criterion of the J_c measurement [14] [15] and sometimes use an inappropriate criterion to determine the threshold current I_{th} from which J_c is calculated [16]. A conventional method can obtain J_c values that differ from the accurate values by 10 % to 20 % [15]. It is thus ~~necessary~~ important to establish standard test methods to precisely measure the local critical current density and its distribution, to which all involved in the HTS filter industry can refer for quality control of the HTS films. Background knowledge on the inductive J_c measurements of HTS thin films is summarized in Annex A.

In these inductive methods, AC magnetic fields are generated with AC currents $I_0\cos\omega t$ in a small coil mounted just above the film, and J_c is calculated from the threshold coil current I_{th}, at which full penetration of the magnetic field to the film is achieved [17]. For the inductive method using third-harmonic voltages U_3, U_3 is measured as a function of I_0, and the I_{th} is determined as the coil current I_0 at which U_3 starts to emerge. The induced electric fields E in the superconducting film at $I_0 = I_{th}$, which are proportional to the frequency f of the AC current, can be estimated by a simple Bean model [14]. A standard method has been proposed to precisely measure J_c with an electric-field criterion by detecting U_3 and obtaining the n-value (index of the power-law E-J characteristics) by measuring I_{th} precisely at various frequencies [14] [15] [18] [19]. This method not only obtains precise J_c values, but also facilitates the detection of degraded parts in inhomogeneous specimens, because the decline of n-value is more ~~remarkable~~ noticeable than the decrease of J_c in such parts [15]. It is noted that this standard method is excellent for assessing homogeneity in large-area HTS films, although the relevant parameter for designing microwave devices is not J_c, but the surface resistance. For application of large-area superconducting thin films to SFCLs, knowledge on J_c distribution is vital, because J_c distribution significantly affects quench distribution in SFCLs during faults.

The International Electrotechnical Commission (IEC) draws attention to the fact that it is claimed that compliance with this document may involve the use of a patent ~~concerning the determination of the E-J characteristics by inductive J_c measurements as a function of frequency, given in the Introduction, Clause 1, Clause 4 and 5.1~~. IEC takes no position concerning the evidence, validity, and scope of this patent right.

[1] Numbers in square brackets refer to the Bibliography.

The holder of this patent right has assured IEC that s/he is willing to negotiate licences ~~free of charge~~ under reasonable and non-discriminatory terms and conditions with applicants throughout the world. In this respect, the statement of the holder of this patent right is registered with IEC. Information may be obtained from the patent database available at http://patents.iec.ch.

~~Name of holder of patent right:~~
~~National Institute of Advanced Industrial Science and Technology~~

~~Address:~~
~~Intellectual Property Planning Office, Intellectual Property Department~~
~~1-1-1, Umezono, Tsukuba, Ibaraki Prefecture, Japan~~

Attention is drawn to the possibility that some of the elements of this document may be the subject of patent rights other than those ~~identified above~~ in the patent database. IEC shall not be held responsible for identifying any or all such patent rights.

~~ISO (www.iso.org/patents) and IEC (http://patents.iec.ch) maintain on-line data bases of patents relevant to their standards. Users are encouraged to consult the data bases for the most up-to-date information concerning patents.~~

SUPERCONDUCTIVITY –

Part 17: Electronic characteristic measurements – Local critical current density and its distribution in large-area superconducting films

1 Scope

This part of IEC 61788 ~~describes~~ specifies the measurements of the local critical current density (J_c) and its distribution in large-area high-temperature superconducting (HTS) films by an inductive method using third-harmonic voltages. The most important consideration for precise measurements is to determine J_c at liquid nitrogen temperatures by an electric-field criterion and obtain current-voltage characteristics from its frequency dependence. Although it is possible to measure J_c in applied DC magnetic fields [20] [21], the scope of this document is limited to the measurement without DC magnetic fields.

This technique intrinsically measures the critical sheet current that is the product of J_c and the film thickness d. The range and measurement resolution for $J_c d$ of HTS films are as follows.

– $J_c d$: from 200 A/m to 32 kA/m (based on results, not limitation).

– Measurement resolution: 100 A/m (based on results, not limitation).

2 Normative references

The following documents are referred to in the text in such a way that some or all of their content constitutes requirements of this document. For dated references, only the edition cited applies. For undated references, the latest edition of the referenced document (including any amendments) applies.

~~IEC 60050 (all parts), *International Electrotechnical Vocabulary* (available at http://www.electropedia.org<http://www.electropedia.org>)~~

IEC 60050-815, *International Electrotechnical Vocabulary – Part 815: Superconductivity* (available at <http://www.electropedia.org>)

3 Terms and definitions

For the purposes of this document, the terms and definitions given in IEC 60050-815~~:2000~~ apply, some of which are repeated here for convenience.

ISO and IEC maintain terminological databases for use in standardization at the following addresses:

- IEC Electropedia: available at http://www.electropedia.org/
- ISO Online browsing platform: available at http://www.iso.org/obp

3.1
critical current
I_c
maximum direct current that can be regarded as flowing without resistance practically

Note 1 to entry: I_c is a function of magnetic field strength, temperature and strain.

[SOURCE: IEC 60050-815:~~2000~~2015, 815-~~03~~12-01]

3.2
critical current criterion
I_c criterion
criterion to determine the critical current, I_c, based on the electric field strength, E, or the resistivity, ρ

Note 1 to entry: E = 10 µV/m or E = 100 µV/m is often used as electric field criterion, and $\rho = 10^{-14}$ Ω · m or $\rho = 10^{-13}$ Ω · m is often used as resistivity criterion. ~~("E = 10 V/m or E = 100 V/m" in the current edition is mistaken and is scheduled to be corrected in the second edition).~~

[SOURCE: IEC 60050-815:~~2000~~2015, 815-~~03~~12-02]

3.3
critical current density
J_c
electric current density at the critical current using either the cross-section of the whole conductor (overall) or of the non-stabilizer part of the conductor if there is a stabilizer

Note 1 to entry: The overall current density is called engineering current density (symbol: J_e).

[SOURCE: IEC 60050-815:~~2000~~2015, 815-~~03~~12-03]

3.4
transport critical current density
J_{ct}
critical current density obtained by a resistivity or a voltage measurement

[SOURCE: IEC 60050-815:~~2000~~2015, 815-~~03~~12-04]

3.5
***n*-value**
<superconductor> exponent obtained in a specific range of electric field strength or resistivity when the voltage/current $U(I)$ curve is approximated by the equation $U \propto I^n$

[SOURCE: IEC 60050-815:~~2000~~2015, 815-~~03~~12-10]

4 Requirements

The critical current density J_c is one of the most fundamental parameters that describe the quality of large-area HTS films. In this document, J_c and its distribution are measured non-destructively via an inductive method by detecting third-harmonic voltages $U_3\cos(3\omega t + \theta)$. A small coil, which is used both to generate AC magnetic fields and detect third-harmonic voltages, is mounted just above the HTS film and used to scan the measuring area. To measure J_c precisely with an electric-field criterion, the threshold coil currents I_{th}, at which U_3 starts to emerge, are measured repeatedly at different frequencies and the E-J characteristics are determined from their frequency dependencies.

The target relative combined standard uncertainty in the method used to determine the absolute value of J_c is less than 10 %. However, the target uncertainty is less than 5 % for the purpose of evaluating the homogeneity of J_c distribution in large-area superconducting thin films.

5 Apparatus

5.1 Measurement equipment

Figure 1 shows a schematic diagram of a typical electric circuit used for the third-harmonic voltage measurements. This circuit is comprised of a signal generator, power amplifier, digital multimeter (DMM) to measure the coil current, band-ejection filter to reduce the fundamental wave signals and lock-in amplifier to measure the third-harmonic signals. It involves the single-coil approach in which the coil is used to generate an AC magnetic field and detect the inductive voltage. This method can also be applied to double-sided superconducting thin films ~~without hindrance~~ with no obstacles. In the methods proposed here, however, there is an additional system to reduce harmonic noise voltages generated from the signal generator and the power amplifier [14]. In an example of Figure 1, a cancel coil of specification being the same as the sample coil is used for cancelling. The sample coil is mounted just above the superconducting film, and a superconducting film with a $J_c d$ sufficiently larger than that of the sample film is placed below the cancel coil to adjust its inductance to that of the sample coil. Note that the inductance of the sample coil decreases by 20 % to 30 % due to the superconducting shielding current when it is mounted on a superconducting film. Both coils and superconducting films are immersed in liquid nitrogen (a broken line in Figure 1). Other optional measurement systems are described in Annex B.

NOTE In this circuit, coil currents of about 0,1 A (RMS) and power source voltages of > 6 V (RMS) are needed to measure the superconducting film of $J_c d \approx 10$ kA/m while using coil 1 or 2 of Table 2. A precision power amplifier~~, such as NF: HSA4011,~~ with sufficiently high power is ~~necessary~~ used to supply such large currents and voltages.

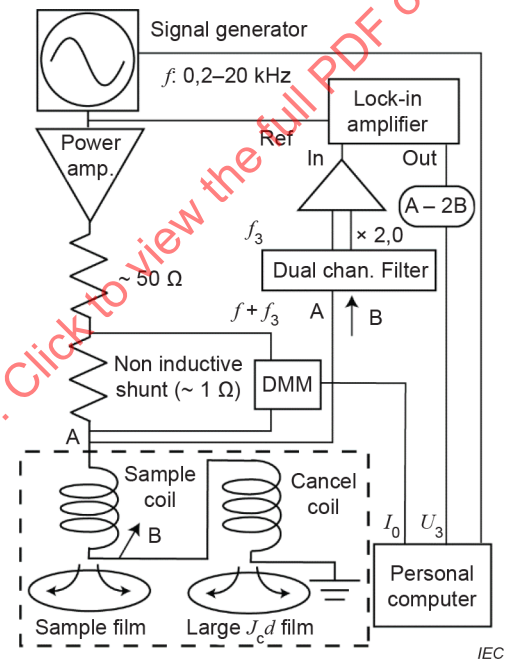

NOTE The broken line surrounds elements immersed in liquid nitrogen.

Figure 1 – Diagram for an electric circuit used for inductive J_c measurement of HTS films

5.2 Components for inductive measurements

5.2.1 Coils

Currently available large-area HTS films are deposited on areas as large as about 25 cm in diameter, while films about 5 cm in diameter are commercially used to prepare microwave filters [22]. Larger $YBa_2Cu_3O_7$ (YBCO) films, about 10 cm in diameter and 2,7 cm × 20 cm, were used to fabricate fault current limiter modules [3] [4] [5]. For the J_c measurements of such films, the appropriate outer diameter of the sample coils ranges from 2 mm to 5 mm. The requirement for the sample coil is to generate as high a magnetic field as possible at the upper surface of the superconducting film, for which flat coil geometry is suitable. Typical specifications are as follows.

a) Inner winding diameter D_1: 0,9 mm, outer diameter D_2: 4,2 mm, height h: 1,0 mm, 400 turns of a 50 µm diameter copper wire.

b) D_1: 0,8 mm, D_2: 2,2 mm, h: 1,0 mm, 200 turns of a 50 µm diameter copper wire.

5.2.2 Spacer film

Typically, a polyimide film with a thickness of 50 µm to 125 µm is used to protect the HTS films. The coil has generally some protection layer below the coil winding, which also insulates the thin film from Joule heat in the coil. The typical thickness is 100 µm to 150 µm, and the coil-to-film distance Z_1 is kept to be 200 µm.

5.2.3 Mechanism for the set-up of the coil

To maintain a prescribed value for the spacing Z_1 between the bottom of the coil winding and the film surface, the sample coil should be pressed to the film with sufficient pressure, typically exceeding about 0,2 MPa [18]. Techniques to achieve this are to use a weight or spring, as shown in Figure 2. The system schematically shown in the figure left is used to scan a wide area of the film. Before the U_3 measurement the coil is initially ~~moved~~ raised up to some distance, moved laterally to the target position, and then ~~moved~~ lowered down and pressed to the film. An appropriate pressure should be determined so that too high pressure does not damage the bobbin, coil, HTS thin film or the substrate. It is reported that the YBCO deposited on biaxially-textured pure Ni substrate was degraded by transverse compressive stress of about 20 MPa [23].

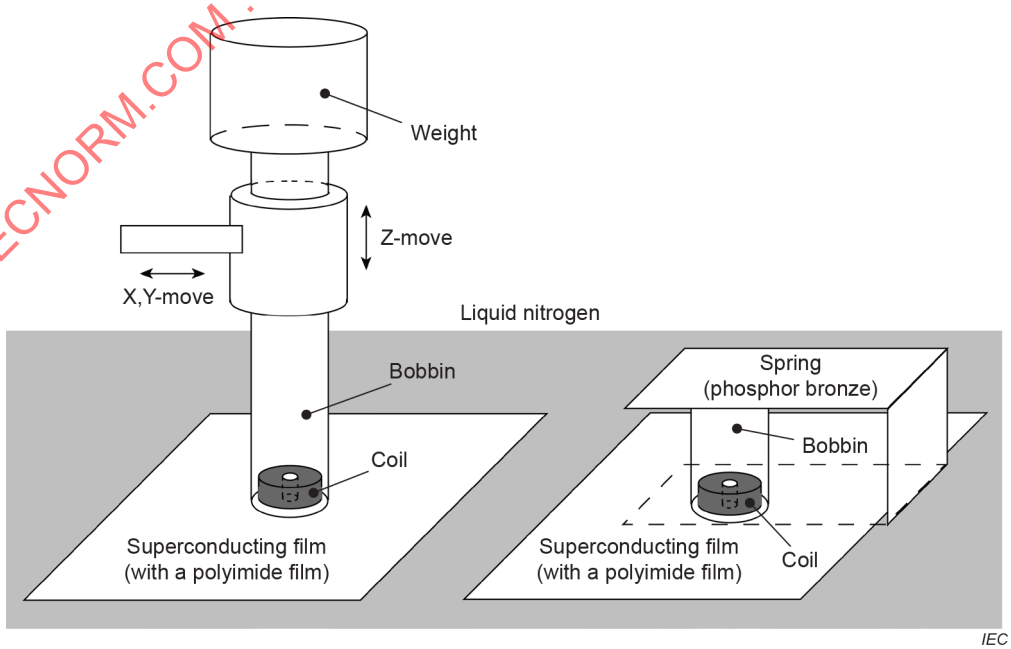

Figure 2 – Illustration showing techniques to press the sample coil to HTS films

5.2.4 Calibration wafer

A calibration wafer is used to determine the experimental coil coefficient k' described in Clause 6. It is made by using a homogeneous large-area (typically about 5 cm diameter) YBCO thin film. It consists of bridges for transport measurement and an inductive measurement area (Figure 3). Typical dimensions of the transport bridges are 20 µm to 70 µm wide and 1 mm to 2 mm long, which were prepared either by UV photolithography technique or by laser etching [24]. In the transport bridge area shown in Figure 3, a transport current can be passed from current terminal 1 to another current terminal 3 through the bridge "a". In this case, terminals 2 and 12 are used as voltage terminals. Similarly, a transport current can be passed from current terminal 1 to another current terminal (5, 7, 9 or 11) through the bridge "b", "c", "d" or "e". In this case, terminals 4, 6, 8 or 10, and 12 are used as voltage terminals.

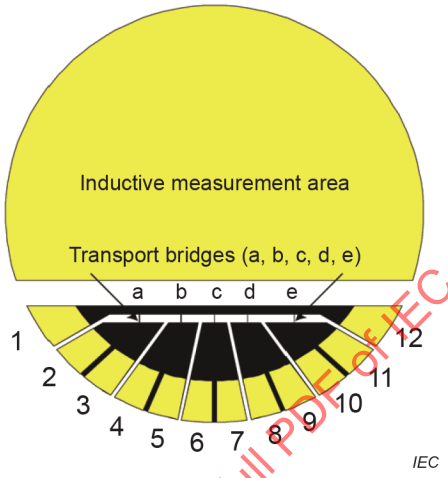

Figure 3 – Example of a calibration wafer used to determine the coil coefficient

6 Measurement procedure

6.1 General

The procedures used to determine the experimental coil coefficient k' and measure the J_c of the films under test are described as follows, with the meaning of k' expressed in Clause A.5.

6.2 Determination of the experimental coil coefficient

6.2.1 Calculation of the theoretical coil coefficient k

Calculate the theoretical coil coefficient $k = J_c d/I_{th}$ from

$$k = F_m, \tag{1}$$

where F_m is the maximum of $F(r)$ that is a function of r, the distance from the central axis of the coil whose inner diameter is D_1, outer diameter is D_2 and height is h (Figure 4). The coil-factor function $F(r) = -2H_r(r, t)/I_0 \cos\omega t = 2H_0/I_0$ is obtained by

$$F(r) = \frac{N}{2\pi S}\int_{R_1}^{R_2} \mathrm{d}r' \int_0^{2\pi} \mathrm{d}\theta \int_{Z_1}^{Z_2} \mathrm{d}z \frac{r' z \cos\theta}{(z^2 + r^2 + r'^2 - 2rr'\cos\theta)^{3/2}}, \tag{2}$$

where ~~N is the number of windings, $S = (R_2 - R_1)h$ is the cross-sectional area, $R_1 = D_1/2$ is the inner radius, $R_2 = D_2/2$ is the outer radius of the coil, Z_1 is the coil-to-film distance, and $Z_2 = Z_1 + h$ [17]. The derivation of the Equation (2) is described in A.3~~.

$H_r(r, t)$ is the radial component of the magnetic field generated by the sample coil at a upper surface of the superconducting film, N is the number of turns in the sample coil, $R_1 = D_1/2$ is the inner radius, $R_2 = D_2/2$ is the outer radius of the coil, $S = (R_2 - R_1)h$ is the cross-sectional area, Z_1 is the coil-to-film distance, and $Z_2 = Z_1 + h$ [17]. The explanation of Equations (1) and (2) is given in Clause A.3.

A simple method to obtain k is as follows.

a) Calculate the magnetic-field amplitude $H_0(r) = H_r(r, t = 0)$ as a function of r at a position below the coil with a distance Z_1 when a current of I_0 = 1 mA is passed in the sample coil (Figure 5).

b) Obtain the (local) maximum value of $H_0(r)$ when r is changed near $r \approx (R_1 + R_2)/2$.

c) The maximum value of $H_0(r)$ should have a unit of A/m, then the doubled value divided by I_0 (= 1 mA) becomes k (unit: 1/mm). Note that the magnetic field arising from the image coil (i.e. from the shielding current flowing in the superconducting film) cancels out the perpendicular component H_z, and the parallel component H_r doubles. The image coil and its magnetic field generation are shown by the broken lines in Figure 5.

d) For the calculation of coil magnetic fields, a free web site may be used; for example, http://www.sc.kyushu-u.ac.jp/~kajikawa/javascript/field_and_potential-e.html
(the calculation of this site is based on a paper entitled "Calculation of Magnetic Field Distribution of Solenoid Coil by Computer" [25].[2]

Some examples of the theoretical coil coefficient k for typical sample coils are shown in Table 1 with the specifications.

2 This information is given for the convenience of users of this document and does not constitute an endorsement by IEC.

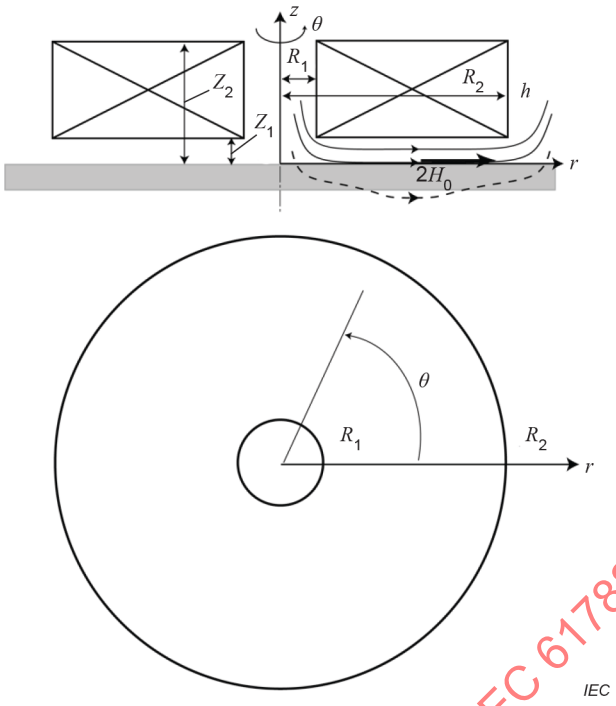

Figure 4 – Illustration of the sample coil and the magnetic field during measurement

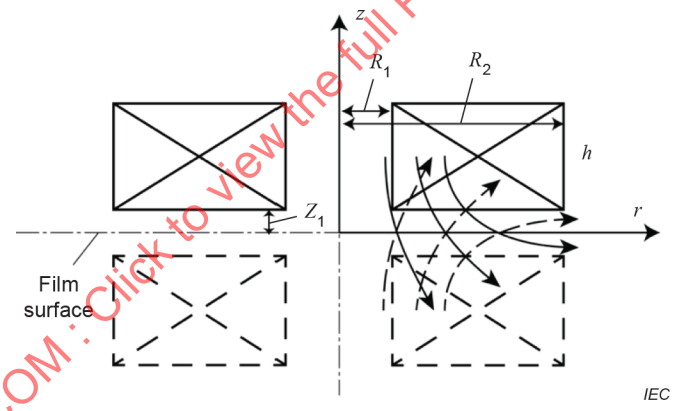

NOTE The image coil and its magnetic field generation are shown by the broken line.

Figure 5 – Illustration of the sample coil and its magnetic field generation

Table 1 – Specifications and theoretical coil coefficients k of sample coils

	D_1 mm	D_2 mm	h mm	Turns	k 1/mm	r at $F(r) = F_m$ mm
A1	0,8	2,2	1,0	200	62,9	0,74
A2	0,9	2,9	1,0	300	92,2	0,95
A3	1,0	3,6	1,0	400	117,4	1,15
A4	1,0	4,3	1,0	500	135,2	1,35
A5	1,0	4,9	1,0	600	151,5	1,52
A6	1,0	3,6	1,5	600	136,0	1,17
B1	1,0	4,3	1,0	150	34,4	1,35
B2	1,0	5,4	1,0	200	41,9	1,67
B3	1,0	6,5	1,0	250	47,9	1,98
B4	1,0	7,6	1,0	300	52,6	2,31
B5	1,5	5,4	1,5	300	51,5	1,68
Coils A1 to A6 are made of 50-µm-diameter copper wires (coil-to-film distance Z_1 = 0,2 mm), and coils B1 to B5 are made of 100-µm-diameter copper wires (coil-to-film distance Z_1 = 0,33 mm).						

6.2.2 Transport measurements of bridges in the calibration wafer

a) Measure the E-J characteristics of the transport bridges of the calibration wafer by a four-probe method, and obtain the power-law E-J characteristics,

$$E_t = A_{0t} \times J^n. \quad (3)$$

b) Repeat the measurement for at least three different bridges. Three sets of data (n = 20,5 to 23,8) measured for three bridges are shown in the upper (high-E) part of Figure 6.

6.2.3 U_3 measurements of the calibration wafer

a) Measure U_3 in the inductive measurement area of the calibration wafer as a function of the coil current with three or four frequencies, and obtain the experimental I_{th} using a constant-inductance criterion; namely, ~~$U_3/fI_0 = 2\pi L_c$~~ $U_3/fI_{th} = 2\pi L_c$. The criterion L_c should be as small as possible within the range with sufficiently large signal-to-noise (S/N) ratios, in order to use the simple Equation (4) for the electric-field calculation (7.1 c) and Clause C.2)~~. An example of the measurement is shown in Figure 6 with $2\pi L_c$ = 2 µΩ•sec.~~

b) Repeat the measurement for at least three different points of the film.

6.2.4 Calculation of the E-J characteristics from frequency-dependent I_{th} data

a) Calculate J_{c0} (= kI_{th}/d) and the average E induced in the superconducting film at the full penetration threshold (when $J_c = J_{c0}$) by

$$E_{avg\text{-}U_3} \approx 2{,}04\mu_0 fd^2 J_c = 2{,}04\mu_0 kfdI_{th} \quad \text{~~} E_{avg} \approx 2{,}04\mu_0 fd^2 J_c = 2{,}04\mu_0 kfdI_{th}\text{~~}, \quad (4)$$

from the obtained I_{th} at each frequency using the theoretical coefficient k calculated in 6.2.1. The derivation of Equation (4) is described in Clause A.4.

b) Obtain the E-J characteristics, and the electric fields E_i induced in the superconducting film can be approximated as

$$E_i = A_{0i} \times J^n \,, \tag{5}$$

from the relation between ~~E_{avg}~~ $E_{avg\text{-}U_3}$ and J_{c0}, and plot them in the same figure where the transport E-J characteristics data were plotted. Broken lines in Figure 6 show three sets of data measured at different points of the film. Transport data and U_3 inductive data do not yet match at this stage.

6.2.5 Determination of the k' from J_{ct} and J_{c0} values for an appropriate E

a) Choose an appropriate electric field that is within (or near to) both the transport E-J curves and the inductive E-J curves, such as 200 μV/m in Figure 6.

b) At this electric field, calculate both the transport critical current densities J_{ct} and the inductive J_{c0} values from Equation (3) and Equation (5), respectively.

c) Determine the experimental coil coefficient k' by $k' = (J_{ct}/J_{c0})k$, where J_{ct} and J_{c0} indicate the average values of obtained J_{ct} and J_{c0} values, respectively. If the J_c ($= k'I_{th}/d$) values are plotted against ~~$E_{avg} = 2{,}04\mu_0 kfdI_{th}$~~ $E_{avg\text{-}U_3} = 2{,}04\mu_0 kfdI_{th}$, the E-J characteristics from the U_3 measurement match the transport data well (Figure 6).

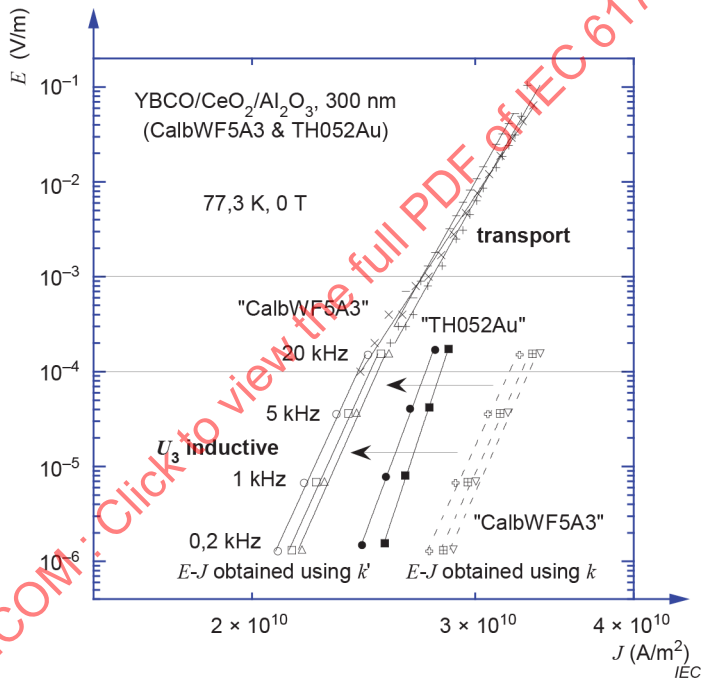

NOTE Broken lines show three sets of data measured at different points of the film.

Figure 6 – E-J characteristics measured by a transport method and the U_3 inductive method

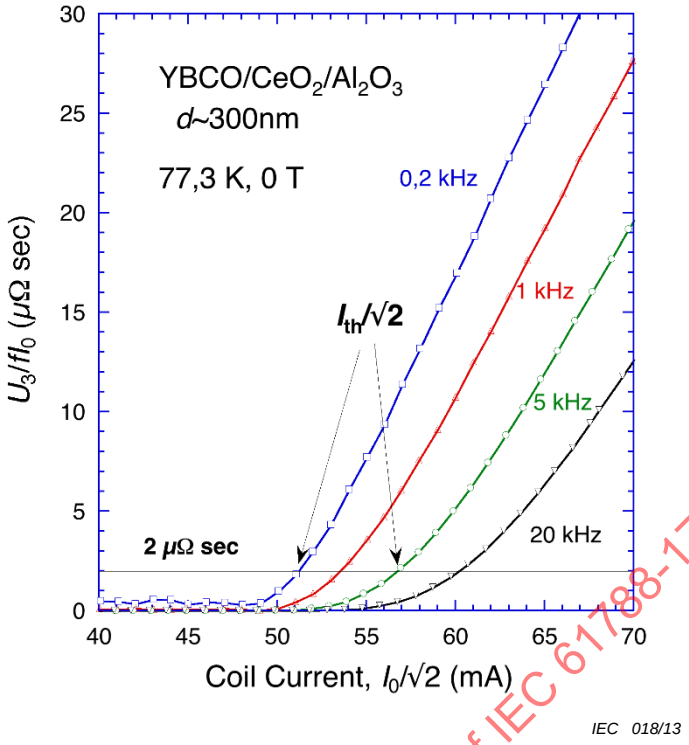

~~**Figure 6 – Example of the normalized third-harmonic voltages (U_3/If_0) measured with various frequencies**~~

6.3 Measurement of J_c in sample films

a) Measure U_3 with two, three or four frequencies in sample films, and obtain I_{th} with the same criterion L_c as used in 6.2.3.

b) Use the obtained experimental coil coefficient k' to calculate J_c (= $k'I_{th}/d$) at each frequency, and obtain the relation between J_c and ~~E_{av}~~ $E_{avg\text{-}U_3}$ (= $2{,}04\mu_0 kfdI_{th}$) using k because of the underestimation as mentioned in 7.1 c). An example of the E-J characteristics is also shown in Figure 6, measured for a sample film (TH052Au, solid symbols) with n-values (36,0 and 40,4) exceeding those of the calibration wafer (n = 28,0 to 28,6).

c) From the obtained E-J characteristics, calculate the J_c value with an appropriate electric-field criterion, such as E_c = 100 μV/m.

d) Measurement with three or four frequencies is beneficial to check the validity of the measurement and sample by checking the power-law E-J characteristics. Measurement with two frequencies can be used for routine samples in the interests of time.

6.4 Measurement of J_c with only one frequency

As mentioned in Clause 1 and Clause 3, ~~J_c is a function of electric field, and~~ it is recommended to determine J_c with a constant electric-field criterion using a multi-frequency approach through procedures described in 6.2 and 6.3, because a supercurrent flowing in a superconductor is a function of electric field. However, one frequency measurement is sometimes desired for simplicity and inexpensiveness. In this case, the J_c values are determined with variable electric-field criteria as specified in the following procedures.

a) Calculate the theoretical coil coefficient k as described in 6.2.1.

b) Obtain the E-J characteristics of the transport bridges of the calibration wafer (Equation (3)) through the procedures of 6.2.2.

c) Measure U_3 in the inductive measurement area of the calibration wafer as a function of the coil current with one frequency, and obtain the experimental I_{th} using a constant-inductance criterion; namely, $U_3/fI_0 = 2\pi L_c$. The criterion L_c should be as small as possible within the range with sufficiently large S/N ratios, in order to use the simple Equation (4) in 6.2.4 for the electric-field calculation. Calculate J_{c0} (= kI_{th}/d) and the average E induced in the superconducting film at the full penetration threshold by Equation (4). Repeat the measurement for at least three different points of the film, and obtain average J_{c0} and $E_{avg\text{-}U_3}$.

d) Using the transport E-J characteristics of Equation (3), calculate J_{ct} for the average $E_{avg\text{-}U_3}$ obtained in c).

e) Determine the experimental coil coefficient k' by $k' = (J_{ct}/J_{c0})k$.

f) Measure U_3 with the same frequency in sample films, and obtain I_{th} with the same criterion L_c as used in c). Calculate J_c (= $k'I_{th}/d$) using the obtained experimental coil coefficient k'. Calculate also ~~E_{avg}~~ $E_{avg\text{-}U_3}$ with Equation (4), and this value should be accompanied by each J_c value.

6.5 Examples of the theoretical and experimental coil coefficients

Some examples of the theoretical and experimental coil coefficients (k and k') for typical sample coils are shown in Table 2 with the specifications and recommended criteria for the I_{th} determination, $2\pi L_c = U_3/fI_0$. Note that the k' depends on the criterion L_c. ~~Coil 1 is wound with a 50 µm diameter, self-bonding polyurethane enameled round copper winding wire, and coils 2 and 3 are wound with a 50 µm diameter, polyurethane enameled round copper winding wire.~~ Coils 1 and 2 are wound with a 50 µm diameter, polyurethane enamelled round copper winding wire, and coil 3 is wound with a 50 µm diameter, self-bonding polyurethane enamelled round copper winding wire. Measured resistances at 77,3 K and calculated self-inductances when a superconducting film is placed below the coil are also shown. The coil-to-film distance Z_1 is fixed at 0,2 mm. The images of coils 1 and 3 are shown in Figure 7, and the coil-factor functions $F(r)$ for the three coils show that the peak magnetic field occurs near the mean coil radius (Figure 8).

Table 2 – Specifications and coil coefficients of typical sample coils

	~~D_1~~ ~~mm~~	~~D_2~~ ~~mm~~	~~h~~ ~~mm~~	~~Turns~~	~~k~~ ~~1/mm~~	~~k'~~ ~~1/mm~~	~~U_3/fI_0~~ ~~µΩ•sec~~	~~R~~ ~~Ω~~	~~L~~ ~~mH~~
~~1~~	~~0,9~~	~~4,2~~	~~1,0~~	~~400~~	~~106,6~~	~~82,2~~	~~2~~	~~4,1~~	~~0,165~~
~~2~~	~~1,0~~	~~3,6~~	~~1,0~~	~~400~~	~~117,4~~	~~89,1~~	~~2~~	~~3,4~~	~~0,163~~
~~3~~	~~0,8~~	~~2,2~~	~~1,0~~	~~200~~	~~63,2~~	~~47,0~~	~~0,6~~	~~1,6~~	~~0,028~~

	D_1 mm	D_2 mm	h mm	Turns	k 1/mm	k' 1/mm	U_3/fI_0 µΩ·s	R Ω	L mH
1	0,8	2,2	1,0	200	62,9	47,0	0,6	1,6	0,028
2	1,0	3,6	1,0	400	117,4	89,1	2	3,4	0,163
3	0,9	4,2	1,0	400	106,6	82,2	2	4,1	0,165

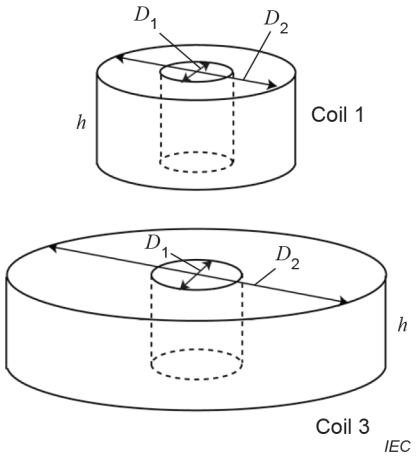

Figure 7 – Illustration of coils 1 and 3 in Table 2

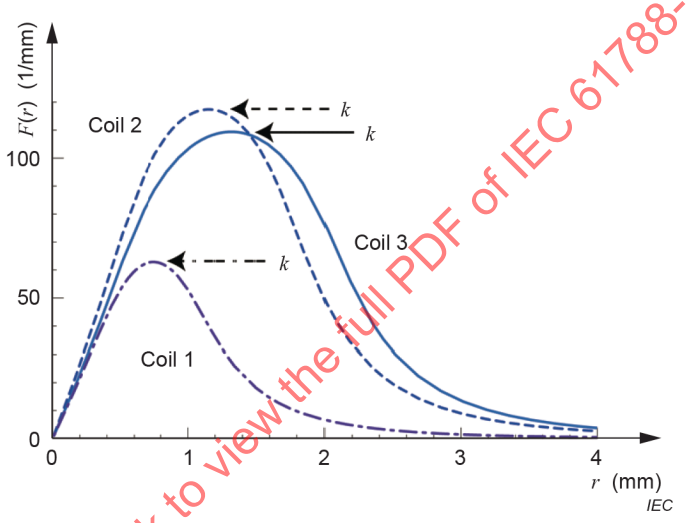

Figure 8 – The coil-factor function $F(r) = 2H_0/I_0$ calculated for the three coils

7 Uncertainty in the test method

7.1 Major sources of systematic effects that affect the U_3 measurement

The most significant systematic effect on the U_3 measurement is due to the deviation of the coil-to-film distance Z_1 from the prescribed value. Because the measured value $J_c d$ in this technique is directly proportional to the magnetic field at the upper surface of the superconducting film, the deviation of the spacing Z_1 directly affects the measurement. The key origins of the uncertainty are listed in a) to c) below. ~~Note that the general concept of the "uncertainty" is summarized in Annex C.~~

a) Inadequate pressing of the coil to the film

As the measurement is performed in liquid nitrogen, the polyimide film placed above the HTS thin film becomes brittle and liquid nitrogen may enter the space between the polyimide and HTS films. Thus, sufficient pressure is ~~necessary~~ needed to keep the polyimide film flat and avoid the deviation of Z_1. An experiment has shown that the required pressure is about 0,2 MPa [18]. Here it is to be noted that thermal contraction of polyimide films at the liquid nitrogen temperature is less than ~~0,002 × (300 − 77) ≈ 0,45 %~~ 0,008 × (300 − 77) ≈ 1,78 %,

which leads to negligible values of ~~0,2 µm to 0,6 µm~~ 0,9 µm to 4,5 µm compared with the total coil-to-film distance (about 200 µm) [26].

b) Ice layer formed between the coil and polyimide film

The liquid nitrogen inevitably contains powder-like ice. If the sample coil is moved to scan the large-area HTS film area for an extended period, an ice layer is often formed between the polyimide film and the sample coil, which increases the coil-to-film distance Z_1 from the prescribed value. As shown later in 7.2, this effect reduces coil coefficients (k and k'), and the use of uncorrected k' results in an overestimate in J_c. Special care should be taken to keep the measurement environment as dry as possible. If the measurement system is set in an open (ambient) environment, the J_c values measured after an extended period of time become sometimes greater than those measured before, and the overestimation was as large as 6 % when measured after one hour. If the measurement system is set in almost closed environment and the ambient humidity is kept less than about 5 %, such effect of ice layers can be avoided. We can check this effect by confirming reproducibility. If the same J_c values are obtained after an extended period, it proves that there is negligible effect of ice layers. These two systematic effects (a) and b)) are not considered in the estimate of the uncertainty in the experimental coil coefficient k' in 7.3 and Clause C.1, because they can be eliminated by careful measurements.

c) Underestimation of the induced electric field E by a simple Bean model

The calculation of average induced electric fields ~~E_{avg}~~ $E_{avg\text{-}U_3}$ in the superconducting film via Equation (4) is sufficiently accurate provided the magnetic-field penetration below the bottom of the film can be neglected. However, considerable magnetic fields penetrate below the film when the experimental threshold current I_{th} is determined and detectable U_3 has emerged. It was pointed out that the rapid magnetic-field penetration below the film at $I_0 = I_{th}$ may cause a considerable increase of the induced electric field and that the E calculated by Equation (4) might be significantly underestimated [27]. However, several experimental results have shown that the relative standard uncertainty from this effect is usually less than 5 %. The detail is described in Clause C.2.

7.2 Effect of deviation from the prescribed value in the coil-to-film distance

Because the magnetic field arising from the coil depends on the coil-to-film distance Z_1, the coil coefficient also depends on Z_1. Figure 9 shows the Z_1 dependence of the theoretical coil coefficient k calculated from Equations (1) and (2). The theoretical coil coefficient k normalized by k_0 is plotted as the function of Z_1, where k_0 is the theoretical coil coefficient for Z_1 = 0,2 mm. Dimensions of coils 1, 2, and 3 are listed in Table 2. The relative effect of deviation on k of coil ~~1~~ 3 is about 2,6 %, when Z_1 = 0,2 mm ± 0,02 mm. Provided the deviation of Z_1 is small (e.g. ≤ 20 %), the deviated experimental coil coefficient k' is proportional to k. Some experimental results that support this are described in Clause C.3. Therefore, use Figure 9 to estimate the systematic effect on k', if the deviated distance can be reasonably estimated.

The effect of the coil inclination to the superconducting film was theoretically investigated [28]. It was found that the theoretical coil coefficient k decreases approximately 7 % when the sample coil (D_1 = 1,0 mm, D_2 = 3,6 mm, h = 1 mm) is inclined 4 % and the distance between the coil and the superconducting thin film is increased.

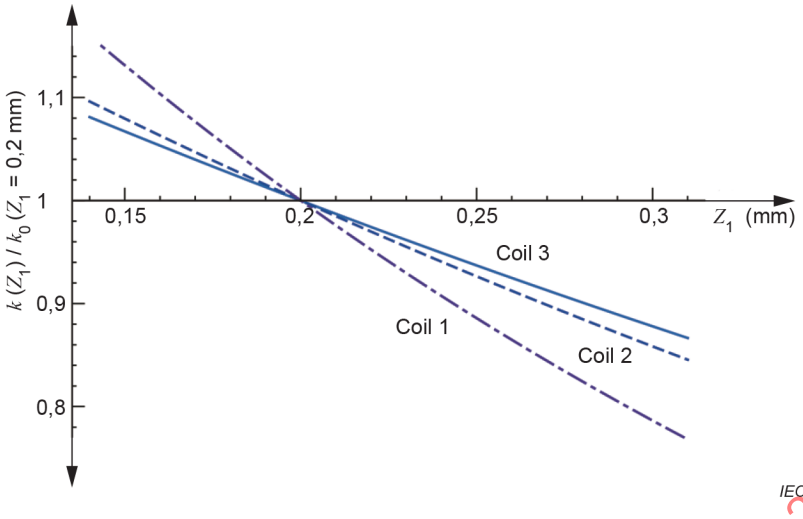

Figure 9 – The coil-to-film distance Z_1 dependence of the theoretical coil coefficient k

7.3 Uncertainty in the experimental coil coefficient and the obtained J_c

Since the proposed method uses a standard sample (the calibration wafer) to determine the experimental coil coefficient k' that directly affects the measured J_c values, the uncertainty in k' is one of the key factors affecting the uncertainty in the measurement, and the homogeneity of the large-area thin film used in the calibration wafer is an important source of such uncertainty. The experimental coil coefficient k' is calculated by $k' = (J_{ct}/J_{c0})k$ at an appropriate electric field, where J_{ct} is the critical current density measured by the transport method and $J_{c0} = kI_{th}/d$ measured by the inductive method (6.2.5). ~~An example of the evaluation of the uncertainty of k' for the coil 1 (Table 1) was shown in D.1. The result is $k' = (J_{ct}/J_{c0})k = (2{,}5878/3{,}4437) \times 109{,}4 = 82{,}2$ mm^{-1} with the combined standard uncertainty of $u_c(k') = 2{,}4$ mm^{-1} (2,93 %).~~ An example of the evaluation of the uncertainty in k' for the coil 3 (Table 2) is shown in Clause C.1. The result is $k' = (J_{ct}/J_{c0})k = \{(2{,}587\ 8 \times 10^{10}$ A/m$^2)/(3{,}355\ 6 \times 10^{10}$ A/m$^2)\} \times 106{,}6$ mm$^{-1} = 82{,}2$ mm^{-1} with the combined standard uncertainty in $u_c(k') = 2{,}4$ mm^{-1} (2,93 %). It has been demonstrated that the uncertainty in the transport J_{ct} dominates the combined standard uncertainty in k'.

The uncertainty originating from the underestimation of ~~E_{avg}~~ $E_{avg\text{-}U_3}$ by a simple Bean model (Equation (4)) is evaluated in Clause C.2. The relative standard uncertainty (Type B) is evaluated to be $u_B = 6{,}6/\sqrt{3}$ % = 3,8 % for a typical specimen with $n = 25$. In contrast to these Type-B uncertainties, Type-A uncertainty in J_c, originating from the experimental uncertainty in the electric U_3 measurement, is much smaller, typically about 0,3 %, as shown in Clause C.4. The uncertainty in k' and that from the underestimation of ~~E_{avg}~~ $E_{avg\text{-}U_3}$ dominate the combined standard uncertainty in the absolute value of J_c, and the relative combined standard uncertainty was 4,7 % for a typical $DyBa_2Cu_3O_7$ (DyBCO) sample film (Clause C.5). This is well below the target value of 10 %. Note that for the purpose of evaluating the homogeneity of J_c distribution in large-area superconducting thin films, the uncertainty in k' does not contribute to the uncertainty in J_c distribution, provided the same sample coil is used. Therefore, the relative standard uncertainty should be less than the target uncertainty of 5 %.

7.4 Effects of the film edge

Figure 8 shows that substantial magnetic fields exist, even outside the coil area, which induce shielding currents in the superconducting film. Therefore, the coil ~~must~~ needs to be apart from the film edge for the precise measurement. The original paper by Claassen *et al*. recommended that the outer diameter of the coil should be less than half of the film width to neglect the edge effect [10]. However, recent numerical calculation with the finite element method indicated that correct measurements can be made when the film width is as small as 6 mm for a coil with an outer diameter of 5 mm and for Z_1 = 0,2 mm [29]. The experimental results described in Clause C.6 have shown that precise measurements can be made for either of coils 2 or 3 (Table 2) when the outside of the coil is more than 0,3 mm apart from the film edge. With the uncertainty of 0,1 mm to 0,2 mm in the coil setting in mind, the outside of the coil should be more than 0,5 mm apart from the film edge when coils with an outer diameter of 2 mm to 5 mm are used.

7.5 Specimen protection

Moisture and water sometimes react with the Ba atoms in the YBCO film and cause the superconducting properties to deteriorate. If YBCO films are still used for some purpose after the measurement, they should be warmed up in a moisture-free environment, e.g. a vacuum or He gas to avoid degradation. Some protection measure can also be provided for the specimens. A thin organic coating, with thickness less than several micrometres, does not affect the measurements and can subsequently be removed; thus it can be used for protection.

8 Test report

8.1 Identification of test specimen

The test specimen shall be identified, if possible, by the following:

a) name of the manufacturer of the specimen;
b) classification;
c) lot number;
d) chemical composition of the thin film and substrate;
e) thickness and roughness of the thin film;
f) manufacturing process technique.

8.2 Report of J_c values

The J_c values shall be reported with the electric-field criterion, E_c. If possible, the n-values, the indices of the power-law E-J characteristics, shall be reported together. It is known that the measurement of n-values facilitates the detection of degraded segments within a large-area HTS film [15].

8.3 Report of test conditions

The following test conditions shall be reported:

a) temperature (atmospheric pressure, or the pressure of liquid nitrogen);
b) DC magnetic fields (if applied);
c) test frequencies;
d) possible effects of the ice layer;
e) specifications of the sample coil;
f) thickness of the spacer film.

Annex A
(informative)

Additional information relating to Clauses 1 to 8

A.1 Comments on other methods for measuring the local J_c of large-area HTS films

There are several AC inductive methods for the nondestructive measurement of local J_c of large-area superconducting thin films [10] [11] [12] [13] [17], in which some detect third-harmonic voltages $U_3\cos(3\omega t + \theta)$ [10] [11] [17] and others use only the fundamental voltage [12] [13]. In these inductive methods, AC magnetic fields are generated with AC currents $I_0\cos\omega t$ in a small coil mounted just above the film, and J_c is calculated from the threshold coil current I_{th}, at which full penetration of the AC magnetic field to the film is achieved [14]. When $I_0 < I_{th}$, the magnetic field below the film is completely shielded, and the superconducting film is regarded as a mirror image coil reflected through the upper surface of the film, carrying the same current but in the opposite direction. The response of the superconducting film to $I_0\cos\omega t$ is linear and no third-harmonic voltage is induced in the coil.

For the case of the U_3 inductive method, U_3 starts to emerge at $I_0 = I_{th}$, when the superconducting shielding current reaches the critical current and its response becomes nonlinear [17]. In the other methods that use only the fundamental voltage, to detect the breakdown of complete shielding when the critical current is reached, penetrated AC magnetic fields are detected by a pickup coil mounted just below the film [12] or a change of mutual inductance of two adjacent coils is measured [13]. In all these inductive J_c measurements, the scheme is common in that the AC magnetic field $2H_0\cos\omega t$ at the upper surface of the film is measured at the full penetration threshold. We obtain J_c because the amplitude of the full penetration field $2H_0$ equals $J_c d$ [17]. The electric field E induced in the superconductor can be calculated with the same Equation (4) [14], and a similar procedure to that described in Clause 6 can be used for the precise measurement.

Another inductive magnetic method using Hall probe arrays has been commercialized to measure local J_c of long coated conductors [30] [31]. In this method magnetic field profiles are measured in applied DC magnetic field, and the corresponding current distribution is calculated. This method can also be applied to rectangular large-area HTS films having widths less than several centimetres, and has better spatial resolution over AC inductive methods using small coils.

A.2 Requirements

As the third-harmonic voltages are proportional to the measuring frequency, higher frequencies are desirable to obtain a better S/N ratio. However, there is a limitation due to the frequency range of the measuring equipment (lock-in amplifier and/or filter) and to excessive signal voltages induced in the sample coil when a large $J_c d$ film is measured. It is recommended to use a frequency from 1 kHz to 20 kHz for a film with small $J_c d$ (≤ 1 kA/m), and a frequency from 0,2 kHz to 8 kHz for a film with large $J_c d$ (≥ 20 kA/m). Measurements over a wide frequency range are desirable to obtain the current-voltage characteristics in a wide electric-field range. For the general purpose of the J_c measurement, however, one order of frequency range is sufficient to obtain the n-value and measure J_c precisely.

In this document, the measurement temperature is limited to liquid nitrogen temperatures, namely 77,35 K at 1 013 hPa and 65,80 K at 200 hPa, because a refrigerant is needed to cool the sample coil that generates Joule heat. When measuring at variable temperatures in a gas atmosphere, further investigations are necessary.

The U_3 inductive method is applicable not only to large-area HTS films deposited on insulating substrates (sapphire, MgO, etc.), but also to coated conductors with metallic substrates. However, if the coated conductors have thick metallic protective layers (Ag or Cu) and their thickness exceeds about 10 µm, certain measures are needed to avoid the skin effect. One technique involves limiting measuring frequencies to a sufficiently low extent (e.g. about 8 kHz).

A.3 Theory of the third-harmonic voltage generation

Here we present the response of a superconducting film to a current-carrying coil mounted above the film (Figure A.1) [17]. A superconducting film of thickness d, infinitely extended in the xy plane, is situated at $-d < z < 0$, where the upper surface is at $z = 0$ in the xy plane and the lower surface is at $z = -d$. A drive coil is axially symmetric with respect to the z-axis, and the coil occupies the area of $R_1 < r < R_2$ and $Z_1 < z < Z_2$ in the cylindrical coordinate (r, θ, z). The coil consists of a wire of ~~winding number N~~ N turns, which carries a sinusoidal drive current $I_d(t) = I_0 \cos\omega t$ along the θ direction. Responding to the magnetic field produced by the coil, the shielding current flows in the superconducting film. The sheet current K_θ (i.e. the current density integrated over the thickness, $-d < z < 0$) in the superconducting film plays crucial roles in the response of the film, and $|K_\theta|$ cannot exceed its critical value, $J_c d$.

The response of the superconducting film is detected by measuring the voltage $U(t)$ induced in the coil, and $U(t)$ is generally expressed as the Fourier series,

$$U(t) = \sum_{n=1}^{\infty} U_n \cos(n\omega t + \theta_n) \,. \tag{A.1}$$

The fundamental voltage U_1 is primarily determined by the coil impedance. The even harmonics, U_n for even n, is generally much smaller than the odd harmonics, U_n for odd n. The third-harmonic voltage, U_3, is the key, because U_3 directly reflects the nonlinear response (i.e. information on $J_c d$) of the superconducting film.

The coil produces an axially symmetric magnetic field, and its radial component H_r at the upper surface of the superconducting film ($z = 0$) is obtained by

$$H_r(r,t) = -H_0 \cos\omega t = -(I_0 / 2) F(r) \cos\omega t \,. \tag{A.2}$$

The coil-factor function $F(r)$ is determined by the configuration of the coil as

$$F(r) = \frac{N}{2\pi S} \int_{R_1}^{R_2} \mathrm{d}r' \int_0^{2\pi} \mathrm{d}\theta \int_{Z_1}^{Z_2} \mathrm{d}z \frac{r' z \cos\theta}{(z^2 + r^2 + r'^2 - 2rr'\cos\theta)^{3/2}} \,, \tag{A.3}$$

where $S = (R_2 - R_1)(Z_2 - Z_1)$ is the cross-sectional area of the coil. The $F(r)$ generally has a maximum $F_m > 0$ at $r = r_m$ [where r_m is roughly close to $(R_1 + R_2)/2$], and $F(0) = F(\infty) = 0$.

When $0 < I_0 < I_{th}$, the magnetic field arising from the coil does not penetrate below the film ($z < -d$). In such cases, the magnetic field distribution above the film ($z > 0$) is simply obtained by the mirror-image technique. The magnetic field arising from the image coil (i.e. from the shielding current flowing in the superconducting film) cancels out the perpendicular component H_z, and the parallel component H_r doubles. The sheet current K_θ in the superconducting film is therefore obtained by $K_\theta(r, t) = 2H_r(r, t) = -I_0F(r)\cos\omega t$. Because of the linear response of the superconducting film for $0 < I_0 < I_{th}$, the voltage induced in the coil contains no harmonics.

Note that the amplitude of the sheet current density, $|K_\theta| = 2|H_r| = I_0F(r) \le I_0F_m$, cannot exceed the critical value, J_cd, when $0 < I_0 \le I_{th}$. The threshold current I_{th} is determined such that $|K_\theta| \le I_0F_m$ reaches J_cd when $I_0 = I_{th}$, and is obtained by

$$I_{th} = J_cd\,/F_m = J_cd/k, \tag{A.4}$$

where the (theoretical) coil coefficient is obtained by $k = F_m$.

When $I_0 > I_{th}$, the magnetic field penetrates below the superconducting film, and the nonlinear response of K_θ yields the generation of the harmonic voltages in the coil.

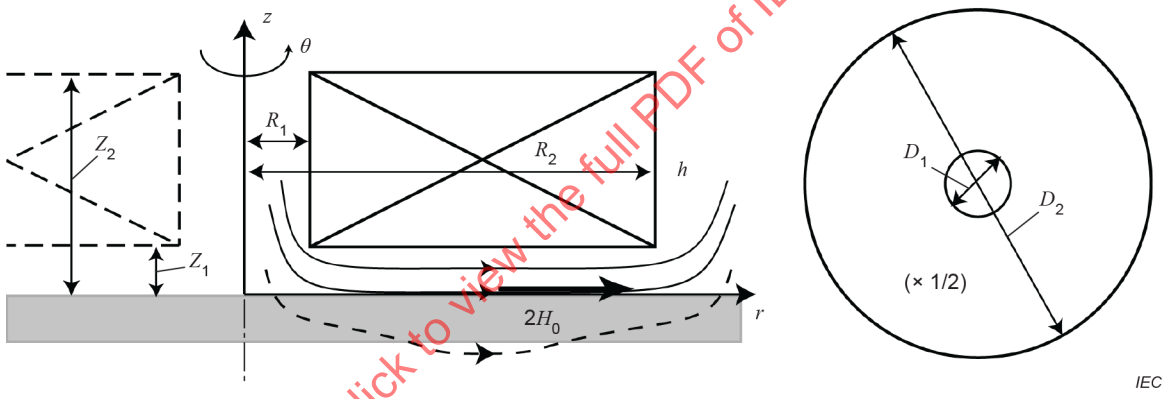

Figure A.1 – Illustration of the sample coil and the magnetic field during measurement

A.4 Calculation of the induced electric fields

Here, we approximate the average E induced in the superconducting film at the full penetration threshold, $I_0 = I_{th}$, using the Bean model [14]. This approximation assumes a semi-infinite superconductor below the xy-plane ($z \le 0$), and the film is regarded as part of this superconductor ($-d \le z \le 0$). When a sinusoidal magnetic field $H_{x0} = 2H_0\cos\omega t$ ($2H_0 = J_cd$) is applied parallel to the x-direction at the surface of the superconductor, the induced E has only the y-component $E_y(z)$, and $E_y(z \le -d)$ is zero because the magnetic fluxes just reach the lower surface of the film ($z = -d$). The $E_y(z)$ is calculated by integrating $-\mu_0(dH_x/dt)$ from $z = -d$ to z, yielding $E_y(z) = -\mu_0\omega dH_0\sin\omega t(1 - \cos\omega t + 2z/d)$. The time-dependent surface electric field, $|E_y(z = 0)|$, peaks at $\omega t = 2\pi/3$, and then, $\max|E_y(0)| = (3\sqrt{3}/4)\,\mu_0\omega dH_0$. Because $\max|E_y(z)|$ peaks at $z = 0$ (the upper surface of the film) and is zero at $z = -d$ (the lower surface of the film), the volume average of $\max|E_y(z)|$ is estimated to be half of $\max|E_y(0)|$,

~~$E_{avg} \approx (3\sqrt{3}\,\pi/4)\,\mu_0 fdH_0 \approx 2{,}04\mu_0 fd^2J_c = 2{,}04\mu_0 kfdI_{th}$~~.

$$E_{\text{avg-}U_3} \approx \left(3\sqrt{3}\pi/4\right)\mu_0 f d H_0 \approx 2{,}04\mu_0 f d^2 J_c = 2{,}04\mu_0 k f d I_{th} \quad \text{(A.5)}$$

For typical parameters of the measurement, f = 1 kHz, d = 250 nm, and J_c = 10^{10} A/m^2, the calculated E is about 2 μV/m.

A.5 Theoretical coil coefficient k and experimental coil coefficient k'

Here, the basic concept concerning the theoretical coil coefficient $k = J_c d/I_{th}$ and the experimental coefficient k' for the case of the U_3 inductive method is explained. When the coil current I_0 equals the threshold current I_{th}, the highest magnetic field below the coil $2H_{0,max} = J_c d$, and the magnetic field just fully penetrates the film. Since $2H_{0,max}$ can be theoretically calculated, we can calculate the theoretical coil coefficient $k = J_c d/I_{th}$. However, the above "true I_{th}" corresponds to the coil current at which infinitesimal U_3 is generated in the coil. Because it is impossible to detect $U_3 \approx 0$ to obtain a "true I_{th}", we need an alternative approach to obtain an "experimental I_{th}" and corresponding experimental coil coefficient k'.

A.6 Scaling of the U_3–I_0 curves and the constant-inductance criterion to determine I_{th}

For convenience, the (experimental) threshold current I_{th} has been often determined by a constant-voltage criterion, e.g. $U_3/\sqrt{2}$ = 50 μV. However, the use of a constant-voltage criterion is problematic. Theoretical analyses on the relationship between I_0 and U_3 showed that there is clear scaling behaviour $U_3/I_{th} = \omega G(I_0/I_{th})$, where G is a scaling function that is determined only by the specifications of the sample coil [11] [17]. This equation implies that the U_3 vs. I_0 curves with various I_{th} values ~~should~~ must collapse to one curve if they are normalized with I_{th}. The inset of Figure A.2 a) clearly shows this scaling behaviour. As the third-harmonic resistance $U_3/I_0 = \omega G(I_0/I_{th})/(I_0/I_{th})$, the U_3/I_0 itself is already normalized (Figure A.2 b)), and it scales with the scaled current I_0/I_{th} (inset of Figure A.2 b)). Because the third-harmonic voltage U_3 is proportional to I_{th}, the determination of I_{th} by a constant-voltage criterion inherently causes a systematic error; namely, the J_c of a sample with $J_c d$ larger (smaller) than the standard sample is underestimated (overestimated) [16]. From the scaling behaviour observed in the third-harmonic resistance U_3/I_0 (Figure A.2 b)), it is demonstrated that the I_{th} should be determined by a constant-resistance criterion, such as U_3/I_0 = 2 mΩ. Furthermore, as the U_3 values are proportional to the measuring frequency, a constant-inductance criterion, such as U_3/fI_0 = 2 μΩ·s, should be used if the U_3 measurements are performed with multiple frequencies [16] [32]. It is also to be noted that such scaling behaviour forms the basis of the $J_c d$ measurement, the procedure for which is described in 6.2 to 6.4 using a standard sample (calibration wafer).

Because a supercurrent flowing in a superconductor is a function of electric field, it is recommended to determine J_c with a constant electric-field criterion using a multi-frequency approach through procedures described in 6.2 and 6.3. An example of the multi-frequency measurement is shown in Figure A.3 with $U_3/fI_0 = 2\pi L_c$ = 2 μΩ·s.

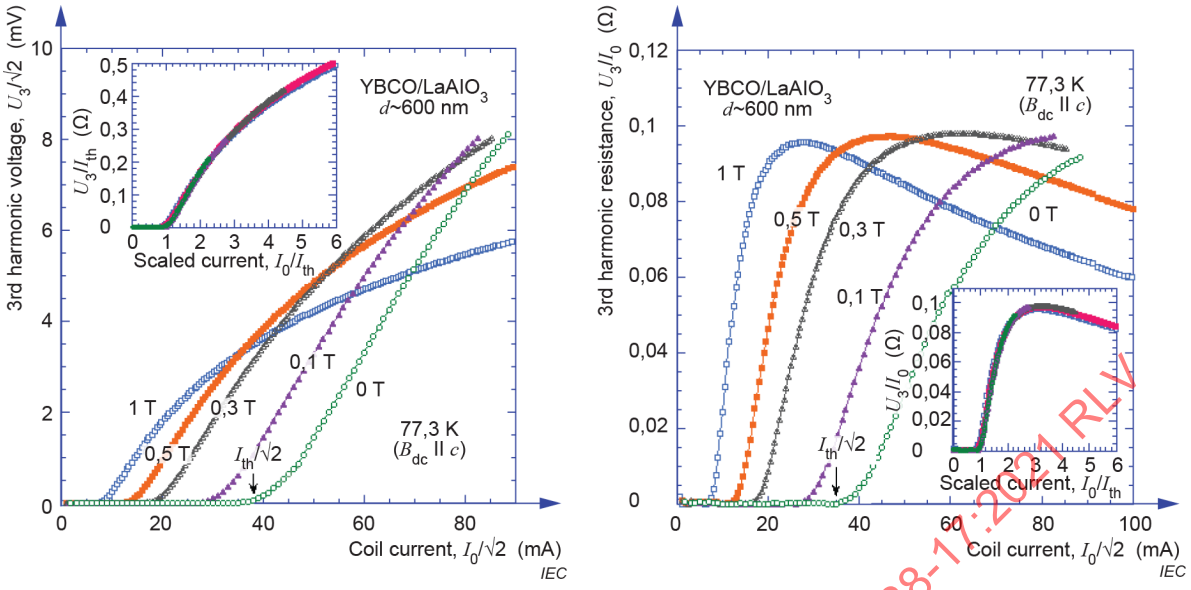

a) U_3 vs. I_0 curves and their scaling

b) U_3/I_0 vs. I_0 curves and their scaling

Figure A.2 – U_3 and U_3/I_0 plotted against I_0 in a YBCO thin film measured in applied DC magnetic fields, and the scaling observed when normalized by I_{th} (insets)

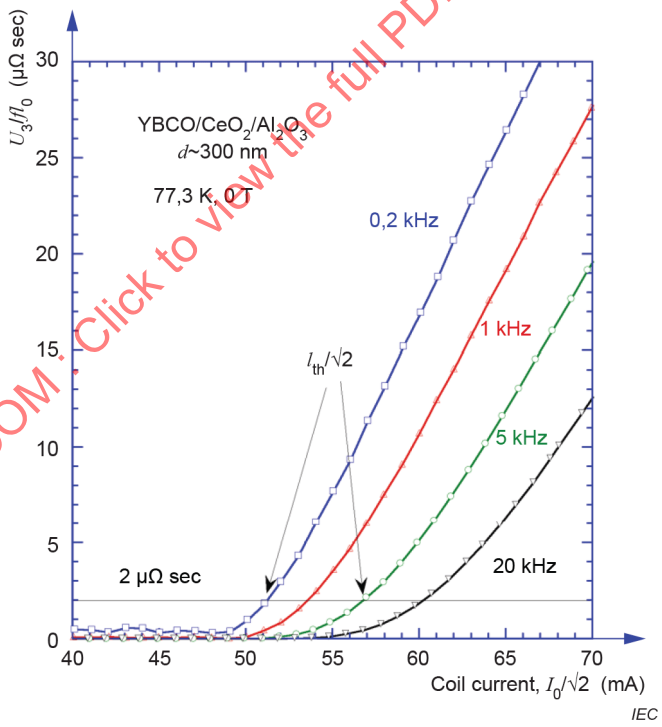

Figure A.3 – Example of the normalized third-harmonic voltages (U_3/fI_0) measured with various frequencies

A.7 Effects of reversible flux motion

The critical state model is frequently used for describing most electromagnetic properties of superconductors. In the critical state model, however, the flux motion is assumed to be completely irreversible. Therefore, if the displacement of flux lines is limited inside the pinning potential, the flux motion includes reversible motion and predictions based on the critical state model are not satisfied. For example, AC energy loss density in multifilamentary Nb-Ti wires with very fine filaments plummets with decreasing filament diameter and deviates from the prediction by the critical state model [33]. The imaginary parts of the AC susceptibility of a superconductor are also predicted to be smaller than the prediction by the critical state model [34]. For the present measurement, it is reported that the critical current density is overestimated at a higher magnetic field [35]. In Clause A.7, the effect of reversible flux motion is described.

When the thickness of the superconducting film is equal to or thinner than the Campbell's AC penetration depth obtained by

$$\lambda_0' = \left(\frac{Ba_f}{2\pi\mu_0 J_c} \right)^{1/2}, \tag{A.6}$$

where a_f is the fluxoid spacing, the reversible flux motion becomes significant. Therefore, the effect of the reversible flux motion is observed at high magnetic fields and/or high temperatures where J_c becomes low. In the present measurement, the magnetic field is limited to a very low level due to the driving coil. λ_0' is estimated to be 140 nm for $J_c = 10^{10}$ A/m^2, B = 0,01 T, and is sufficiently smaller than the typical thin film thickness of 300 nm. However, λ_0' becomes 440 nm for $J_c = 10^9$ A/m^2, meaning the thin film thickness ~~must~~ needs to exceed 880 nm. Thus, it is better to estimate λ_0' from J_c and confirm that the reversible flux motion is not significant in the present measurement, i.e. $\lambda_0' < d$ is satisfied. This estimation of λ_0' is also valid for cases where the DC magnetic field is applied perpendicular to the film surface, while the direction of the AC and DC magnetic fields differ. In this case, λ_0' is known to be estimated from the DC magnetic field [36].

Annex B
(informative)

Optional measurement systems

B.1 Overview

As mentioned in 5.1, an appropriate system to reduce the harmonic noise voltages generated from the signal generator and the power amplifier is necessary for precise U_3 measurements. In the proposed standard method in 5.1 (Figure 1), an additional cancel coil of the same specification as the sample coil, which is placed on a large $J_c d$ superconducting film, is used to compensate for harmonic noise voltages. Although such use of the cancel coil with a large $J_c d$ film is the most recommended method to compensate for the harmonic noise voltages, the use of a cancel coil without a superconducting film is also effective to reduce the noise for U_3 [37]. As the noise for U_3 originating from the power source is proportional to the sample coil impedance, this method is effective if the inductive reactance of the coil is less than the resistance. For example, in a typical coil, e.g. coil ~~No. 1~~ 3 of Table 2 (6.5), the resistance at 77,3 K is similar to the reactance at 3f = 3 kHz, and the reduction of its self-inductance caused by the superconducting shielding current is about 1/3; in this case, the noise for U_3 ~~should~~ is likely to be reduced to less than 20 %. If the harmonic noise voltages are less frequency-dependent, the effect of the noise for U_3 is significant at lower frequencies, because the threshold current I_{th} should be determined with a constant-inductance criterion, $2\pi L_c = U_3/fI_0$ = const. (6.2.3 and 6.4). Therefore, noise cancelling without a large $J_c d$ superconducting film can be used as a simpler method. Some examples of harmonic noise cancelling are shown in Clause B.2.

Another technique to compensate for the harmonic noise voltages is to use variable resistances and variable inductance coils that can emulate the self-inductance and resistance of the sample coil, as shown in Figure B.1 [18] [19]. A pair of coils L_{Va} and L_{Vb} are placed near to each other with the same axis, and their inductances are adjusted to be equal to L_d. The inductances and resistances R_{Va} and R_{Vb} are connected to the sample coil in series, and both impedances Z_a and Z_b of the cancel circuit are adjusted to the impedance Z_d of the sample coil.

The third measure of the noise reduction is to use two coils: a drive coil and another detection coil wound around the former, as shown in Figure B.2. The AC magnetic field is generated with the drive coil, and the third-harmonic voltage induced in the detection coil is measured. As the current does not flow in the detection coil, the contribution from the resistance to the noise for U_3 is eliminated. This method is effective for a small drive coil whose resistance exceeds the inductive reactance. Its major advantage is the simpler circuit compared with the methods using a cancel coil.

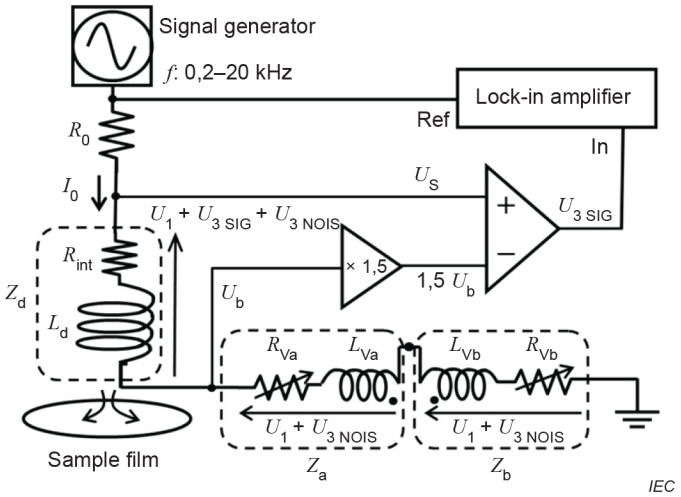

Figure B.1 – Schematic diagram for the variable-*RL*-cancel circuit

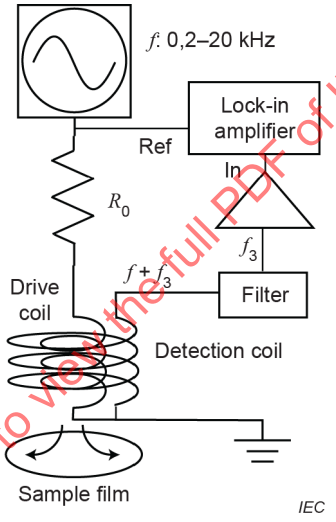

Figure B.2 – Diagram for an electrical circuit used for the two-coil method

B.2 Harmonic noises arising from the power source and their reduction

Figure B.3 shows an example of harmonic noise voltages (f: 0,2 kHz to 20 kHz) generated from a precision signal generator with harmonic distortion ratio less than 0,1 % and a precision power amplifier ~~(NF:1930A and NF:HSA4011)~~, when AC current is passed through an enamelled resistor of 10 Ω. It is seen that the noise is not frequency-dependent when the current is less than 80 mA, which means that this noise affects the measurement more at lower frequencies because the third-harmonic voltage is proportional to the frequency. Figure B.4 shows the effect of the noise reduction in the U_3 measurement with the circuit of Figure 1 having a cancel coil with a superconducting film. The signal "A" was measured without using a cancel coil by short-circuiting B to the ground. The amplitude of "A" initially increases due to the noise, which is equal to the signal "B", slightly decreases and then rapidly increases due to the third-harmonic voltage originating from the nonlinear superconducting response. The slight decrease of U_3 is due to the phase difference between the signal from the superconducting current and the noise [17]. It is seen that the noise is effectively cancelled by the measurement of the "A minus 2B" signal in Figure 1.

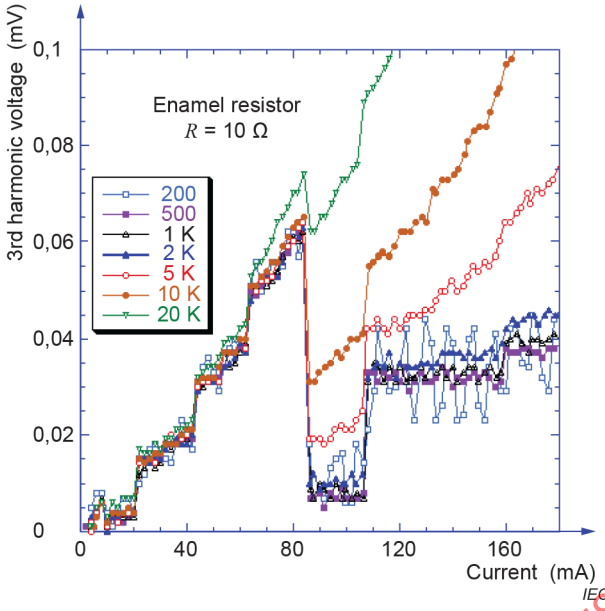

Figure B.3 – Harmonic noises arising from the power source

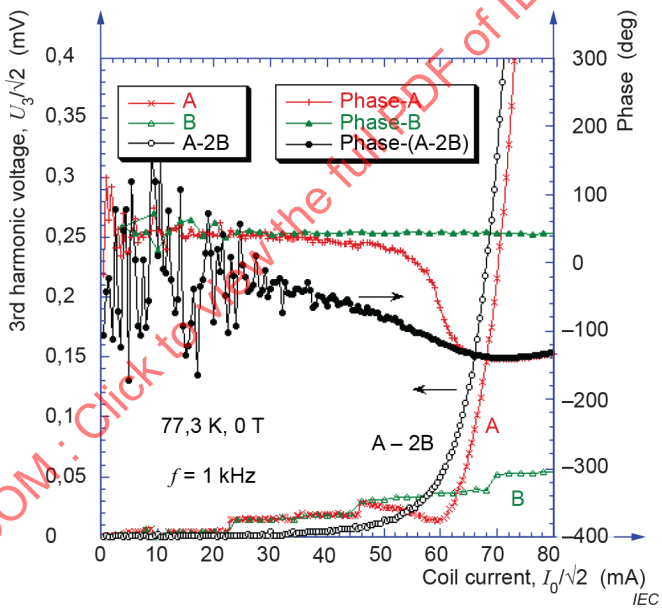

Figure B.4 – Noise reduction using a cancel coil with a superconducting film

The harmonic noise voltages were measured for coil ~~No. 1~~ 3 in Table 2 without any noise reduction system, when a superconducting film with large $J_c d$ was placed below the coil to mimic the measurement without generating any U_3 signal from the superconducting current. Because the threshold current I_{th} is determined by a constant-inductance criterion, such as U_3/fI_0 = 2 μΩ·s, they are plotted in the normalized form, U_3/fI_0 (Figure B.5). It emerges that the use of such a small criterion as $2\pi L_c = U_3/fI_0$ = 2 μΩ·s is not feasible due to significant systematic noise. Such large noise voltages are effectively reduced using a cancel coil with a superconducting film, which enables the use of small criterion like U_3/fI_0 = 2 μΩ·s (Figure B.6). Systematic noise was less than 0,05 μΩ·s even when $I_0/\sqrt{2}$ = 160 mA, which corresponds to $J_c d$ = 18,6 kA/m. As mentioned in Clause B.1, a cancel coil without a superconducting film can also be used for the noise reduction. Figure B.7 shows the noise voltages in a normalized form for coil ~~No. 1~~ 3. The systematic noise level was about 0,1 μΩ·s at 10 kHz or less, which is about

5 % of the recommended criterion of 2 μΩ·s. Typical noise voltages of the measurement with the two-coil system (Figure B.2) were also measured, as shown in Figure B.8. The data were taken with an inner drive coil (D_1 = 1,0 mm, D_2 = 2,8 mm, h = 1,0 mm, 200 turns) and an outer pickup coil (D_1 = 3,0 mm, D_2 = 6,0 mm, h = 1,0 mm, 295 turns). The systematic noise level was about 0,05 μΩ·s at 10 kHz or less, which is about 5 % of an appropriate criterion of 1 μΩ·s.

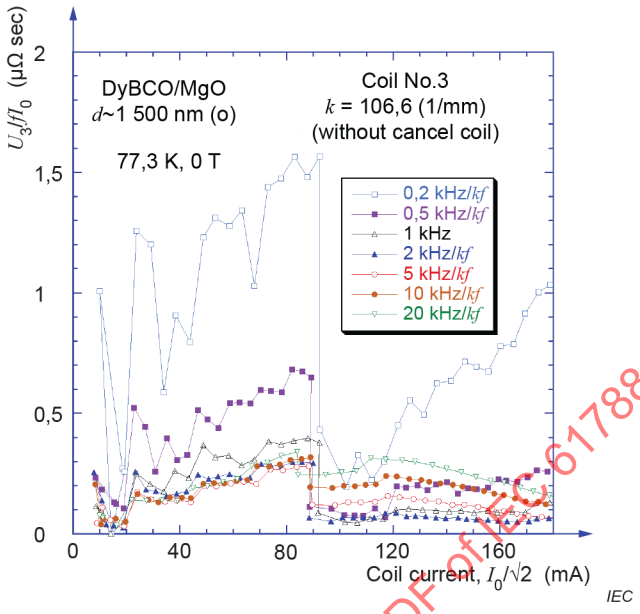

Figure B.5 – Normalized harmonic noises (U_3/fI_0) arising from the power source

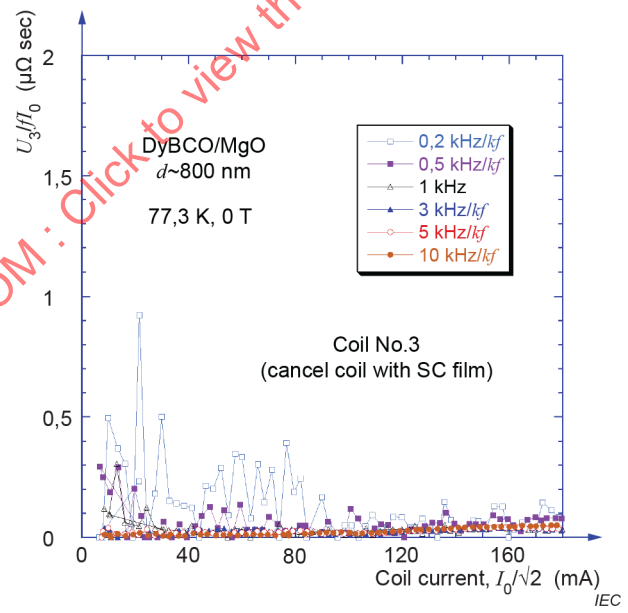

Figure B.6 – Normalized noise voltages after the reduction using a cancel coil with a superconducting film

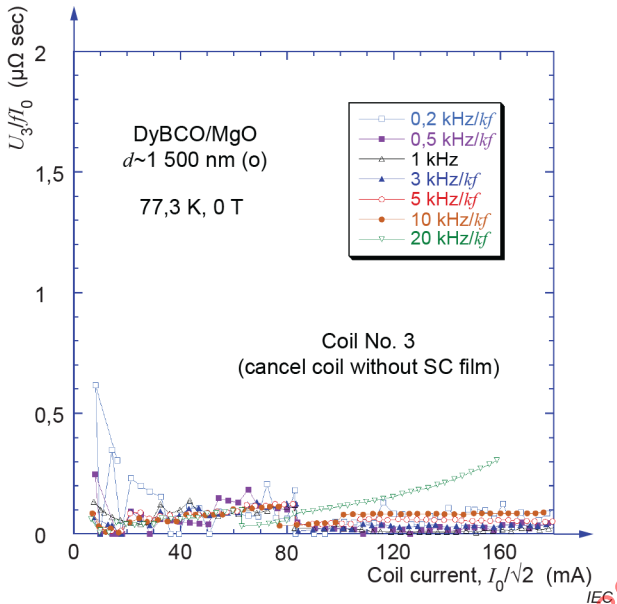

Figure B.7 – Normalized noise voltages after the reduction using a cancel coil without a superconducting film

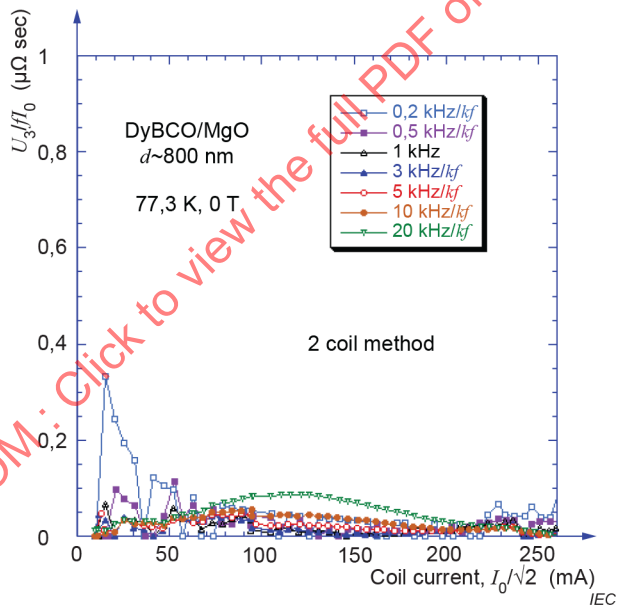

Figure B.8 – Normalized noise voltages with the two-coil system shown in Figure B.2

Annex C
(informative)

Uncertainty considerations

C.1 Overview

In 1995, a number of international standards organizations, including IEC, decided to unify the use of statistical terms in their standards. It was decided to use the word “uncertainty” for all quantitative (associated with a number) statistical expressions and eliminate the quantitative use of “precision” and “accuracy.” The words “accuracy” and “precision” could still be used qualitatively. The terminology and methods of uncertainty evaluation are standardized in the Guide to the Expression of Uncertainty in Measurement (GUM) [1] [3].

It was left to each TC to decide if they were going to change existing and future standards to be consistent with the new unified approach. Such change is not easy and creates additional confusion, especially for those who are not familiar with statistics and the term uncertainty. At the June 2006 TC 90 meeting in Kyoto, it was decided to implement these changes in future standards.

Converting “accuracy” and “precision” numbers to the equivalent “uncertainty” numbers requires knowledge about the origins of the numbers. The coverage factor of the original number may have been 1, 2, 3, or some other number. A manufacturer’s specification that can sometimes be described by a rectangular distribution will lead to a conversion number of $1/\sqrt{3}$. The appropriate coverage factor was used when converting the original number to the equivalent standard uncertainty. The conversion process is not something that the user of the standard needs to address for compliance to TC 90 standards, it is only explained here to inform the user about how the numbers were changed in this process. The process of converting to uncertainty terminology does not alter the user’s need to evaluate their measurement uncertainty to determine if the criteria of the standard are met.

The procedures outlined in TC 90 measurement standards were designed to limit the uncertainty of any quantity that could influence the measurement, based on the Convener’s engineering judgment and propagation of error analysis. Where possible, the standards have simple limits for the influence of some quantities so that the user is not required to evaluate the uncertainty of such quantities. The overall uncertainty of a standard was then confirmed by an interlaboratory comparison.

C.2 Definitions

Statistical definitions can be found in three sources: the GUM, the International Vocabulary of Basic and General Terms in Metrology (VIM)[2], and the NIST Guidelines for Evaluating and Expressing the Uncertainty of NIST Measurement Results (NIST)[3]. Not all statistical terms used in this standard are explicitly defined in the GUM. For example, the terms “relative standard uncertainty” and “relative combined standard uncertainty” are used in the GUM (5.1.6, Annex J), but they are not formally defined in the GUM (see [3]).

C.3 Consideration of the uncertainty concept

Statistical evaluations in the past frequently used the coefficient of variation (COV) which is the ratio of the standard deviation and the mean (N.B. the COV is often called the relative standard

deviation). Such evaluations have been used to assess the precision of the measurements and give the closeness of repeated tests. The standard uncertainty (SU) depends more on the number of repeated tests and less on the mean than the COV and therefore in some cases gives a more realistic picture of the data scatter and test judgment. The example below shows a set of electronic drift and creep voltage measurements from two nominally identical extensometers using same signal conditioner and data acquisition system. The n = 10 data pairs are taken randomly from the spreadsheet of 32 000 cells. Here, extensometer number one (E_1) is at zero offset position whilst extensometer number two (E_2) is deflected to 1 mm. The output signals are in volts.

Table C.1 – Output signals from two nominally identical extensometers

Output signal V	
E_1	E_2
0,00122070	2,33459473
0,00061035	2,33428955
0,00152588	2,33428955
0,00122070	2,33459473
0,00152588	2,33459473
0,00122070	2,33398438
0,00152588	2,33428955
0,00091553	2,33428955
0,00091553	2,33459473
0,00122070	2,33459473

Table C.2 – Mean values of two output signals

Mean ($\overline{x}$) V	
E_1	E_2
0,00119019	2,33441162

$$\overline{X} = \frac{\sum_{i=1}^{n} X_i}{n} \quad [\text{V}] \qquad \text{(C.1)}$$

Table C.3 – Experimental standard deviations of two output signals

Experimental standard deviation (s) V	
E_1	E_2
0,00030348	0,000213381

$$s = \sqrt{\frac{1}{n-1} \cdot \sum_{i=1}^{n} \left(x_i - \overline{x}\right)^2} \quad [\text{V}] \qquad \text{(C.2)}$$

Table C.4 – Standard uncertainties of two output signals

Standard uncertainty (u) V	
E_1	E_2
0,00009597	0,00006748

$$u = \frac{s}{\sqrt{n}} \quad [\mathrm{V}] \tag{C.3}$$

Table C.5 – Coefficient of variations of two output signals

Coefficient of variation (COV) %	
E_1	E_2
25,4982	0,0091

$$COV = \frac{s}{\overline{x}} \tag{C.4}$$

The standard uncertainty is very similar for the two extensometer deflections. In contrast the coefficient of variation COV is nearly a factor of 2800 different between the two data sets. This shows the advantage of using the standard uncertainty which is independent of the mean value.

C.4 Uncertainty evaluation example for TC 90 standards

The observed value of a measurement does not usually coincide with the true value of the measurand. The observed value may be considered as an estimate of the true value. The uncertainty is part of the "measurement error" which is an intrinsic part of any measurement. The magnitude of the uncertainty is both a measure of the metrological quality of the measurements and improves the knowledge about the measurement procedure. The result of any physical measurement consists of two parts: an estimate of the true value of the measurand and the uncertainty of this “best” estimate. The GUM, within this context, is a guide for a transparent, standardized documentation of the measurement procedure. One can attempt to measure the true value by measuring “the best estimate” and using uncertainty evaluations which can be considered as two types: Type A uncertainties (repeated measurements in the laboratory in general expressed in the form of Gaussian distributions) and Type B uncertainties (previous experiments, literature data, manufacturer’s information, etc. often provided in the form of rectangular distributions).

The calculation of uncertainty using the GUM procedure is illustrated in the following example:

a) The user must derive in the first step a mathematical measurement model in the form of identified measurand as a function of all input quantities. A simple example of such model is given for the uncertainty of a force, F_{LC} measurement using a load cell:

$$F_{LC} = W + d_w + d_R + d_{Re}$$

where W, d_w, d_R, and d_{Re} represent the weight of standard as expected, the manufacturer’s data, repeated checks of standard weight/day and the reproducibility of checks at different days, respectively.

Here the input quantities are: the measured weight of standard weights using different balances (Type A), manufacturer’s data (Type B), repeated test results using the digital

electronic system (Type B), and reproducibility of the final values measured on different days (Type B).

b) The user should identify the type of distribution for each input quantity (e.g. Gaussian distributions for Type A measurements and rectangular distributions for Type B measurements).

c) Evaluate the standard uncertainty of the Type A measurements,

$u_A = \frac{s}{\sqrt{n}}$ where, s is the experimental standard deviation and n is the total number of measured data points.

d) Evaluate the standard uncertainties of the Type B measurements:

$u_B = \sqrt{\frac{1}{3} \cdot d_w{}^2 + ...}$ where, d_w is the range of rectangular distributed values

e) Calculate the combined standard uncertainty for the measurand by combining all the standard uncertainties using the expression:

$$u_c = \sqrt{u_A^2 + u_B^2}$$

In this case, it has been assumed that there is no correlation between input quantities. If the model equation has terms with products or quotients, the combined standard uncertainty is evaluated using partial derivatives and the relationship becomes more complex due to the sensitivity coefficients [4, 5].

f) Optional – the combined standard uncertainty of the estimate of the referred measurand can be multiplied by a coverage factor (e. g. 1 for 68 % or 2 for 95 % or 3 for 99 %) to increase the probability that the measurand can be expected to lie within the interval.

g) Report the result as the estimate of the measurand ± the expanded uncertainty, together with the unit of measurement, and, at a minimum, state the coverage factor used to compute the expanded uncertainty and the estimated coverage probability.

To facilitate the computation and standardize the procedure, use of appropriate certified commercial software is a straightforward method that reduces the amount of routine work [6, 7]. In particular, the indicated partial derivatives can be easily obtained when such a software tool is used. Further references for the guidelines of measurement uncertainties are given in [3, 8, and 9].

C.5 Reference documents of Annex C

[1] ISO/IEC Guide 98-3:2008, *Uncertainty of measurement – Part 3: Guide to the expression of uncertainty in measurement* (GUM:1995)

[2] ISO/IEC Guide 99:2007, *International vocabulary of metrology – Basic and general concepts and associated terms (VIM)*

[3] TAYLOR, B.N. and KUYATT, C.E. *Guidelines for Evaluating and Expressing the Uncertainty of NIST Measurement Results*. NIST Technical Note 1297, 1994 (Available at <http://physics.nist.gov/Pubs/pdf.html>)

[4] KRAGTEN, J. Calculating standard deviations and confidence intervals with a universally applicable spreadsheet technique. *Analyst*, 119, 2161-2166 (1994)

[5] EURACHEM / CITAC Guide CG 4 Second edition:2000, *Quantifying Uncertainty in Analytical Measurement*

[6] Available at <http://www.gum.dk/e-wb-home/gw_home.html>

[7] Available at <http://www.isgmax.com/>

[8] CHURCHILL, E., HARRY, H.K., and COLLE, R. *Expression of the Uncertainties of Final Measurement Results*. NBS Special Publication 644 (1983)

[9] JAB NOTE Edition 1:2003, *Estimation of Measurement Uncertainty (Electrical Testing / High Power Testing)*. (Available at <http://www.jab.or.jp>).

Annex C
(informative)

Evaluation of the uncertainty

C.1 Evaluation of the uncertainty in the experimental coil coefficient

The experimental coil coefficient k' is calculated by $k' = (J_{ct}/J_{c0})k$, where J_{ct} is the critical current density measured by using the transport method and $J_{c0} = kI_{th}/d$ measured by using the inductive method, both defined at an appropriate electric field (6.2.5). Typical example data of J_{ct} and J_{c0}, both defined by E_c = 200 µV/m criterion, are shown below, which were used to determine k' for the coil ~~1~~ 3 (Table 2).

J_{ct} (10^{10} A/m^2) for five bridges: 2,578, 2,622, 2,561, 2,566, 2,612.

Mean $\bar{X}$ = 2,587 8, experimental standard deviation s = 0,027 59, standard uncertainty $u_A = s/\sqrt{N}$ = 0,012 339, coefficient of variation ~~COV~~ $c_v = s/\bar{X}$ = 0,010 7 (1,07 %).

J_{c0} (10^{10} A/m^2) for eight points: ~~3,4567, 3,4327, 3,4127, 3,4514, 3,4474, 3,4581, 3,4487, 3,4421~~ 3,368 2, 3,344 8, 3,325 4, 3,363 1, 3,359 2, 3,369 6, 3,360 4, 3,354 0.

~~Mean $\bar{X}$ = 3,4437, s = 0,014915, $u_A = s/\sqrt{N} = 0{,}0052731$, $COV = s/\bar{X}$ = 0,00433 (0,433 %)~~

Mean $\bar{X}$ = 3,355 6, s = 0,014 54, $u_A = s/\sqrt{N}$ = 0,005 141, $c_v = s/\bar{X}$ = 0,004 33 (0,433 %).

The above standard uncertainties of J_{ct} and J_{c0} (Type A measurements) ~~should~~ is likely to be caused from the variation in the critical current density of the YBCO thin film. The standard deviation s and the contribution to $u_c(k')$ in J_{ct} exceed those in J_{c0}, probably because the variation of J_c ~~should~~ is likely to be larger in small transport bridges (20 µm × 1 mm to 70 µm × 1 mm) than in the measurement area of the inductive method, a circle of diameter ≈ 3,9 mm [15]. Similar c_v values for J_{ct} (1,82 %) and J_{c0} (0,346 %) were observed in the measurement that uses the RL-cancel circuit (Figure B.1) [19]. There are other factors that cause the uncertainty in J_{ct}; for example, the uncertainty in the bridge width, that of the transport measurement, etc. The uncertainty from such various causes is regarded here as that from Type B measurements, and the standard uncertainty is calculated from the c_v = 5 % for the transport critical current measurement of Ag-sheathed Bi-2212 and Bi-2223 oxide superconductors [38]. Then, u_B = 2,587 8 × 0,05/$\sqrt{3}$ = 0,074 70 (10^{10} A/m^2). From these data we can draw the following uncertainty budget table (Table C.1), and we obtain the final result: ~~$k' = (J_{ct}/J_{c0})k = (2{,}5878/3{,}4437) \times 109{,}4 = 82{,}2$ mm^{-1} ± 2,4mm^{-1}~~
$k' = (J_{ct}/J_{c0})k$ = (2,587 8/3,355 6) × 106,6 = (82,2 ± 2,4) mm^{-1}. The Type B uncertainty in J_{ct} is seen to dominate the combined standard uncertainty. To promote better understanding of the budget table, the formula of $u_c(k')$ is shown in Equation (C.1):

$$u_c(k') = ((k/J_{c0})^2 u_A(J_{ct})^2 + (k/J_{c0})^2 u_B(J_{ct})^2 + (-kJ_{ct}/J_{c0}^2)^2 u_A(J_{c0})^2)^{1/2}. \quad \text{(C.1)}$$

Table C.1 – Uncertainty budget table for the experimental coil coefficient k'

Factor	Standard uncertainty $u(x_i)$ (10^{10} A/m^2)	Type of measurement	Sensitivity coefficients c_i	Contribution to $u_c(k')$, $\lvert c_i \rvert u(x_i)$
J_{ct}	0,012 339	Type A	31,77 mm^{-1}/(10^{10} A/m^2)	0,392 mm^{-1}
J_{ct}	0,074 70	Type B	31,77 mm^{-1}/(10^{10} A/m^2)	2,373 mm^{-1}
J_{c0}	0,005 273 1	Type A	−23,87 mm^{-1}/(10^{10} A/m^2)	0,126 mm^{-1}
Combined standard uncertainty $u_c(k') = (\Sigma\{c_i u(x_i)\}^2)^{1/2}$				2,409 mm^{-1}

C.2 Uncertainty in the calculation of induced electric fields

In this proposed method, the average E induced in the superconducting film at the full penetration is approximated using the Bean model (Equation (4) in 6.2.4). Although Equation (4) assumes that the magnetic field produced by the coil just reaches the lower surface of the superconducting film (i.e. $I_0 = I_{th}$(theory)), the experimental I_{th} obtained from the U_3 measurements are more than 1,3 times larger than the theoretical I_{th}. When $I_0 > I_{th}$(theory), the magnetic field penetrates below the superconducting film and the induced electric field for $I_0 > I_{th}$ may exceed the theoretical value obtained by Equation (4). The possibility of a large electric field for $I_0 > I_{th}$ is posed in [27]: for simplicity, the response of a superconducting film to a line current has been analytically investigated. When a line current flows in a linear wire above a superconducting film, the threshold current is obtained by $I_{th} = \pi J_c dy_0$, where y_0 is the distance between the linear wire and the superconducting film. The amplitude of the electric field E_{line} induced in the superconducting film is roughly estimated as [27]

$$E_{line} \approx \sqrt{2}\,\mu_0 f I_{th} (I_0/I_{th} - 1) \approx 4{,}44 \mu_0 f J_c dy_0 (I_0/I_{th} - 1) \tag{C.2}$$

for $d/y_0 << I_0/I_{th} - 1 << 1$. The ratio of Equation (C.2) to Equation (4) is estimated to be

~~$E_{line}/E_{avg} \approx 2{,}18\,(y_0/d)\,(I_0/I_{th} - 1) \approx 170,$~~

$$E_{line}/E_{avg\text{-}U_3} \approx 2{,}18\,(y_0/d)(I_0/I_{th} - 1) \approx 170\,, \tag{C.3}$$

where we used $y_0 = Z_1$ = 0,2 mm, d = 250 nm, and I_0/I_{th} = 1,1. This large value of E_{line} arises from the fact that the electric field for $I_0 > I_{th}$ is due to the penetration of magnetic flux perpendicular to the film. Note that the model of the line current in Ref. [27] is too simple to simulate the realistic coil current.

Although the above theory for a line current predicts that induced electric fields can be almost two orders of magnitude larger than those by the simple calculation using a Bean model [Equation (4)], some experimental results have indicated that the underestimation by Equation (4) ~~should~~ is likely to not be so large. For the E-J characteristics of YBCO samples, the slight downward curvature in the wide-range $\log_{10}(E)$ vs. $\log_{10}(J)$ plots is well known. This is a characteristic feature of the vortex-glass phase, in which the J dependent potential barrier diverges at $J \rightarrow 0$ as $U(J) \propto J^{-\mu}$ and the resistance becomes truly zero [39]. Such downward curvature is clearly observed in Figure 6, and the n-values calculated for a lower (higher) E range increase (fall). From the frequency-dependent U_3 measurement using Equation (4), reasonable E-J characteristics and n-values were obtained for YBCO thin films, which match the wide-range E-J characteristics obtained from transport and magnetization measurements well [16] [40]. The perpendicular magnetic-field components are probably cancelled out by

parallel currents, which prevents the emergence of such high electric fields. Provided the inductance criterion for the I_{th} determination is small enough, such as shown in Table 2, the underestimation of ~~E_{avg}~~ $E_{avg\text{-}U_3}$ by Equation (4) ~~should~~ is likely to be at most five times. From the power-law E-J characteristics $E = E_c \times (J/J_c)^n$, we obtain

$$J = J_c \times (E/E_c)^{1/n} , \tag{C.4}$$

where E_c is the electric-field criterion to define J_c. Note that $J = J_c$ when $E = E_c$. If the ~~E_{avg}~~ $E_{avg\text{-}U_3}$ by Equation (4) is underestimated five times, the actual value of E_c should be $5E_c$, when J_c is determined by the criterion ~~E_{avg}~~ $E_{avg\text{-}U_3} = E_c$. This leads to the deviation of J_c, $\Delta J_c = J_c \times (5^{1/n} - 1)$. Therefore, the relative deviations ($\Delta J_c/J_c$) are calculated as 5,5 % (n = 30), 6,6 % (n = 25), and 8,4 % (n = 20). The relative standard uncertainty (Type B, in %) is formulated as

~~$u_B(E_{avg}) = 100(5^{1/n} - 1)/\sqrt{3}$~~

$$u_B\left(E_{avg\text{-}U_3}\right) = 100\left(5^{1/n} - 1\right)\Big/\sqrt{3} \tag{C.5}$$

which becomes u_B (~~E_{avg}~~ $E_{avg\text{-}U_3}$) = 6,6/$\sqrt{3}$ = 3,8 % for a typical specimen with n = 25. For other n-values, u_B = 3,2 % (n = 30), 4,8 % (n = 20), and 6,5 % (n = 15).

C.3 Experimental results on the effect of the deviation of the coil-to-film distance

In 7.2, it is stated that the deviated experimental coil coefficient k' is proportional to k, when the coil-to-film distance Z_1 deviates from the prescribed value but the deviation of Z_1 is small (e.g. ≤ 20 %). Some experimental results supported the estimate of k' based on the change of k (Figure 9). When J_c was measured with coil 2 of Table 2, deviated Z_1' = 0,175 mm but using the unchanged k' led to a J_c value that is 94,5 % of the true J_c measured with correct Z_1 = 0,2 mm. Figure 9 predicts that the experimental coil coefficient $k'(Z_1' = 0{,}175\text{ mm}) = 1{,}063k'(Z_1 = 0{,}2\text{ mm})$, and the experimental result matches the theoretical prediction well. A similar experiment with very large Z_1' = 0,3 mm led to 1,34 times larger J_c, which is slightly larger than the prediction of Figure 9, 1/0,786 = 1,27. This is because the third-harmonic signal also decreases with Z_1 even if the magnetic field is the same. This effect can be neglected when ΔZ_1 is small enough, which can be understood from the nonlinear relation of U_3 against I_0 (Figure A.3 ~~Figure 6~~).

C.4 Examples of the Type-A uncertainties of J_c and n-values, originating from the experimental uncertainty in the U_3 measurement

As was mentioned in Clauses C.1, C.2 and C.3, in the evaluation of the uncertainty in J_c, Type-B uncertainties, namely, the uncertainty in k' and that originating from underestimated E, are generally large, typically > 2 %. In contrast, Type-A uncertainty in J_c, originating from the experimental uncertainty in the electric U_3 measurement, is much smaller. The examples below exhibit repeated measurements of J_c and n-values obtained from the frequency dependence of the experimental I_{th}, under the same conditions in a 250-nm-thick DyBCO thin film (Table C.2). The data in a) were obtained with a frequency set of 0,5 kHz, 2 kHz, 10 kHz, and the data in b) were obtained with a frequency set of 2 kHz, 8 kHz, 35 kHz. The statistics of the data are as follows.

a) J_c (10^{10} A/m^2): Mean $\bar{X}$ = 1,896, s = 0,006 254, $u_A = s/\sqrt{N}$ = 0,001 978, $c_v = s/\bar{X}$ = 0,003 299 (0,33 %) and relative standard uncertainty is $u_A/\bar{X}$ = 0,001 043 (0,10 %).

n: Mean $\bar{X}$ = 23,67, s = 0,577 1, $u_A = s/\sqrt{N}$ = 0,182 5, $c_v = s/\bar{X}$ = 0,024 38 (2,44 %) and relative standard uncertainty is $u_A/\bar{X}$ = 0,007 710 (0,77 %).

b) J_c (10^{10} A/m^2): Mean $\bar{X}$ = 1,904, s = 0,004 498, $u_A = s/\sqrt{N}$ = 0,001 422, $c_v = s/\bar{X}$ = 0,002 362 (0,24 %) and relative standard uncertainty is $u_A/\bar{X}$ = 0,000 746 8 (0,075 %).

n: Mean $\bar{X}$ = 20,40, s = 0,419 4, $u_A = s/\sqrt{N}$ = 0,132 6, $c_v = s/\bar{X}$ = 0,020 56 (2,06 %) and relative standard uncertainty is $u_A/\bar{X}$ = 0,006 500 (0,65 %).

These results indicate that the relative standard uncertainty in n-values (Type A) is less than 1 %, and that Type-A uncertainty in J_c is much smaller, not larger than 0,1 %. Even if the measurement is done only once, such Type-A uncertainties are small; namely, about 2 % for n and about 0,3 % for J_c. This Type-A uncertainty in the n-values directly becomes the uncertainty in n because the shift of the U_3 vs. I_0 curves, as shown in Figure 6, is theoretically predicted for a superconducting film having power-law E-J characteristics and not dependent on any parameters other than n [41]. Note that the n-value measured at higher frequencies, namely, for the higher E region, becomes smaller, reflecting the slight downward curvature of the power-law E-J characteristics, as seen in Figure 6 and explained in Clause C.2. However, the J_c values obtained are the same, 1,90 × 10^{10} A/m^2, because both are defined by the same criterion of E_c = 100 µV/m.

Table C.2 – Examples of repeated measurements of J_c and n-values

Measurement number	a) Measured at 0,5 kHz, 2 kHz, 10 kHz		b) Measured at 2 kHz, 8 kHz, 35 kHz	
	J_c (10^{10} A/m^2)	n	J_c (10^{10} A/m^2)	n
1	1,901	23,51	1,912	19,61
2	1,902	23,35	1,907	20,30
3	1,900	23,53	1,909	20,00
4	1,903	22,77	1,906	20,35
5	1,902	23,09	1,906	19,89
6	1,894	23,76	1,897	20,98
7	1,889	24,51	1,901	20,45
8	1,888	24,41	1,901	20,71
9	1,893	23,43	1,903	20,65
10	1,888	24,29	1,901	20,62

C.5 Evaluation of the uncertainty in the obtained J_c

Typical example data of J_c and n-values of a 250-nm-thick DyBCO sample film (2 cm × 2 cm), defined by E_c = 100 µV/m criterion, are shown below.

J_c (10^{10} A/m^2) (and n-value) for 16 different points: 2,404 (27,5), 2,395 (26,9), 2,396 (27,4), 2,409 (26,6), 2,455 (27,0), 2,432 (26,8), 2,421 (26,6), 2,450 (25,0), 2,423 (26,3), 2,440 (25,2), 2,448 (26,9), 2,481 (26,1), 2,455 (26,1), 2,456 (26,0), 2,450 (26,0), 2,452 (26,0).

Mean $\bar{X}$ = 2,435 4, s = 0,025 025, $u_A = s/\sqrt{N}$ = 0,006 256 3, $c_v = s/\bar{X}$ = 0,010 3 (1,03 %).

The above J_c data were obtained from the U_3 measurements using coil ~~1~~ 3 of Table 2, whose k' = (82,2 ± 2,4) mm^{-1} (Clause C.2). The relative standard uncertainty originating from the experimental uncertainty in the electric U_3 measurement and the distribution of J_c (Type A) is $u_A(J_c)$ = (0,006 256/2,435) × 100 = 0,257 %, which is much smaller than the relative standard uncertainty in k', $u_c(k')/k'$ = (2,409/82,2) × 100 = 2,93 %, and the uncertainty from that of ~~E_{avg}~~ $E_{avg\text{-}U_3}$, u_B(~~E_{avg}~~ $E_{avg\text{-}U_3}$) = 6,39/$\sqrt{3}$ = 3,68 % (n = 26). Finally, the relative combined standard uncertainty is

$$u_c(J_c) = (\{u_c(k')/k'\}^2 + u_B(E_{avg}\ E_{avg\text{-}U_3})^2 + u_A(J_c)^2)^{1/2} = (2{,}93^2 + 3{,}68^2 + 0{,}257^2)^{1/2} = 4{,}71\ \%, \quad \text{(C.6)}$$

which is smaller than the target value of 10 %.

A round-robin test result using the same measuring coil and sample film obtained the following J_c and n-values [19].

J_c (10^{10} A/m^2) (and n-value) for four different points: 2,287 (27,9), 2,291 (26,2), 2,189 (26,2), 2,222 (26,6).

Mean $\bar{X}$ = 2,2472, s = 0,050 082, $u_A = s/\sqrt{N}$ = 0,025 041, $c_v = s/\bar{X}$ = 0,022 3 (2,23 %).

The above J_c data were obtained from the U_3 measurement that uses the RL-cancel circuit (Figure B.1), in which a somewhat large criterion for the I_{th} determination, $2\pi L_c = U_3/fI_0$ = 10 μΩ·s, was used due to the limited S/N ratio [19]. The relative deviation of J_c was (2,435 − 2,247)/2,435 = 0,077 2 = 7,72 %. This exceeds the estimated relative combined standard uncertainty of 4,7 %, probably because the uncertainty from that of $E_{avg\text{-}U3}$ exceeds the estimation in Clause C.2 due to the large $2\pi L_c$. Still, the relative deviation is significantly smaller than the target relative combined standard uncertainty of 10 %.

C.6 Experimental results that reveal the effect of the film edge

The edge effect on the third-harmonic J_c measurements was investigated using a computer-controlled coil-scanning system [15]. A 10-mm-wide YBCO/CeO_2/sapphire thin film with homogeneous J_c distribution was placed side by side between two sapphire substrates of thickness the same to the substrate of the YBCO film, and the coil was scanned as shown by the lines in the diagrams in Figure C.1. Figure C.1 a) exhibits the dependence of the measured J_c on the position of the centre of coil 2 in Table 2 (3,6 mm outer diameter) when Z_1 = 0,2 mm. Correct J_c values were obtained when the coil position was from −2,6 mm to +3,4 mm. To eliminate the edge effect, the necessary distance from the edge is calculated to be {10 − (2,6 + 3,4 + 3,6)}/2 = 0,2 mm. A similar experiment for coil ~~3~~ 1 in Table 2 (2,2 mm outer diameter) indicated that correct J_c values were obtained when the coil position was from −4,0 mm to +3,2 mm (Figure C.1 b)), which leads to the necessary distance of {10 − (4,0 + 3,2 + 2,2)}/2 = 0,3 mm. The result showing an increased necessary distance for coil ~~3~~ 1 rather than coil 2 may be because a larger portion of magnetic fields exists in the outside of the coil area in the case of the former.

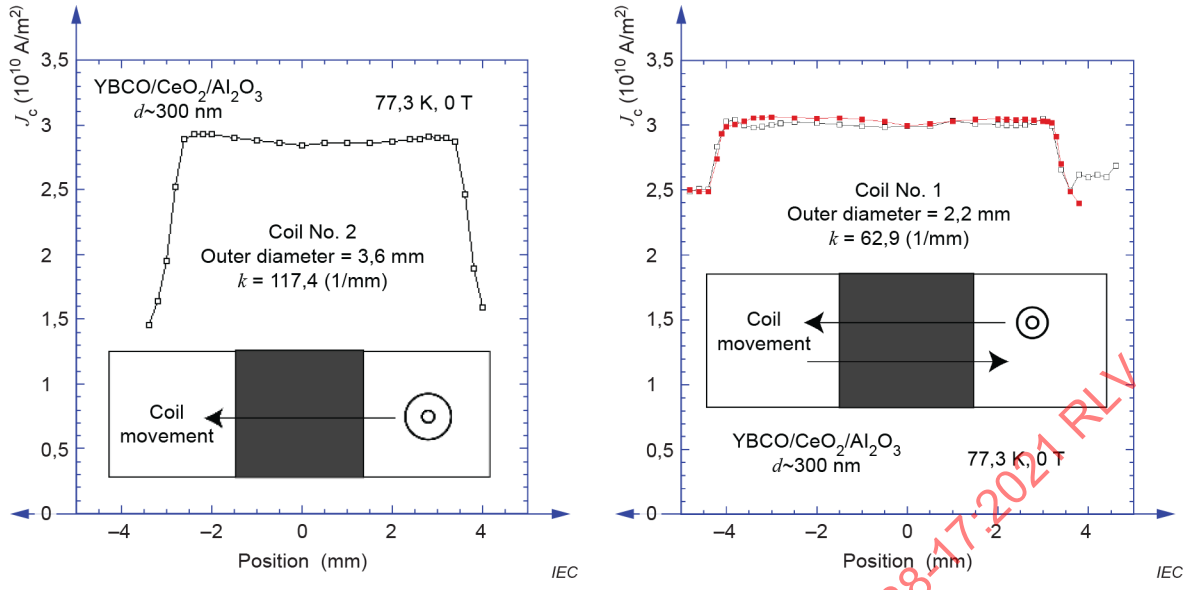

a) For coil 2 in Table 2

b) For coil 1 in Table 2

Figure C.1 – Effect of the coil position against a superconducting thin film on the measured J_c values

Bibliography

[1] LANCASTER, MJ. in Passive Microwave Device Applications of High-Temperature Superconductors, Cambridge University Press, 1997, p. 144

[2] KINDER, H., BERBERICH, P., PRUSSEIT, W., RIEDER-ZECHA, S., SEMERAD, R. and UTZ, B. YBCO film deposition on very large areas up to 20 x 20 cm^2. *Physica C*, 1997, 282–287, p. 107

[3] GROMOLL, B., RIES, G., SCHMIDT, W., KRAEMER, H.-P., SEEBACHER, B., UTZ, B., NIES, R., NEUMUELLER, H.-W., BALTZER, E., FISCHER, S. AND HEISMANN, B. Resistive fault current limiters with YBCO films – 100 kVA functional model. *IEEE Trans. Appl. Supercond.*, 1999, 9, p. 656

[4] HYUN, O.-B., KIM, H.-R., SIM, J., JUNG, Y.-H., PARK, K.-B., KANG, J.-S., LEE, B.-W. and OH, I.-S. 6.6 kV resistive superconducting fault current limiter based on YBCO films. *IEEE Trans. Appl. Supercond.*, 2005, 15, p. 2027

[5] YAMASAKI, H., ARAI, K., KAIHO, K., NAKAGAWA, Y., SOHMA, M., KONDO, W., YAMAGUCHI, I., MATSUI, H., KUMAGAI, T., NATORI N. and HIGUCHI, N. 500 V/200 A fault current limiter modules made of large-area MOD-$YBa_2Cu_3O_7$ thin films with high-resistivity Au-Ag alloy shunt layers. *Supercond. Sci. Technol.*, 2009, 22, p. 125007

[6] YIM, S.-W., KIM, H.-R., HYUN, O.-B., SIM, J., PARK, K. B. AND LEE, B. W. Optimal design of superconducting fault detector for superconductor triggered fault current limiters. *Physica C*, 2008, 468, p. 2072

[7] LEE, B.W., Park, K.B., Sim, J., Oh, I.S., Lee, H.G., Kim, H.R. and Hyun, O.B. Design and Experiments of Novel Hybrid Type Superconducting Fault Current Limiters. *IEEE Trans. Appl. Supercond.*, 2008, 18, p. 624

[8] TOSAKA, T., TASAKI, K., MARUKAWA, K., KURIYAMA, T., NAKAO, H., YAMAJI, M., KUWANO, K., IGARASHI, M., NEMOTO, K. and TERAI, M. Persistent current HTS magnet cooled by cryocooler (4) – persistent current switch characteristics. *IEEE Trans. Appl. Supercond.*, 2005, 15, p. 2293

[9] TOSAKA, T., OHTANI, Y., ONO, M., KURIYAMA, T., MIZUMAKI, S., SHIBUI, M., NAKAMOTO, K., TACHIKAWA, N., MORIKAWA, J., OGAWA, Y. AND YOSHIDA, Z. Development of Persistent-Current Mode HTS Coil for the RT-1 Plasma Device. *IEEE Trans. Appl. Supercond.*, 2006, 16, p. 910

[10] CLAASSEN, JH., REEVES, ME. and SOULEN, Jr. RJ. A contactless method for measurement of the critical current density and critical temperature of superconducting films. *Rev. Sci. Instrum.*, 1991, 62, p. 996

[11] POULIN, GD., PRESTON, JS. and STRACH, T. Interpretation of the harmonic response of superconducting films to inhomogeneous AC magnetic fields. *Phys. Rev. B*, 1993, 48, p. 1077

[12] HOCHMUTH H. and LORENZ, M. Inductive determination of the critical current density of superconducting thin films without lateral structuring. *Physica C*, 1994, 220, p. 209

[13] HOCHMUTH H. and LORENZ, M. Side-selective and non-destructive determination of the critical current density of double-sided superconducting thin films. *Physica C*, 1996, 265, p. 335

[14] YAMASAKI, H., MAWATARI, Y. and NAKAGAWA, Y. Nondestructive determination of current-voltage characteristics of superconducting films by inductive critical current density measurements as a function of frequency. *Appl. Phys. Lett.*, 2003, 82, p. 3275

[15] YAMASAKI, H., MAWATARI, Y., NAKAGAWA, Y., MANABE, T. and SOHMA M. Automatic measurement of the distribution of J_c and n-values in large-area superconducting films using third-harmonic voltages. *IEEE Trans. Appl. Supercond.*, 2007, 17, p. 3487

[16] YAMASAKI, H., MAWATARI, Y. and NAKAGAWA, Y. Precise Determination of the Threshold Current for Third-Harmonic Voltage Generation in the AC Inductive Measurement of Critical Current Densities of Superconducting Thin Films. *IEEE Trans. Appl. Supercond.*, 2005, 15, p. 3636

[17] MAWATARI, Y., YAMASAKI, H. and NAKAGAWA, Y. Critical current density and third-harmonic voltage in superconducting films. *Appl. Phys. Lett.*, 2002, 81, p. 2424

[18] YAMADA, H., MINAKUCHI, T., ITOH, D., YAMAMOTO, T., NAKAGAWA, S., KANAYAMA, K., HIRACHI, K., MAWATARI, Y. and YAMASAKI, H. Variable-RL-cancel circuit for precise J_c measurement using third-harmonic voltage method. *Physica C*, 2007, 451, p. 107

[19] YAMADA, H., MINAKUCHI, T., FURUTA, T., TAKEGAMI, K., NAKAGAWA, S., KANAYAMA, K., HIRACHI, K., OTABE, ES., MAWATARI, Y. and YAMASAKI, H. Wideband-RL-cancel circuit for the *E-J* property measurement using the third-harmonic voltage method. *J. Phys.: Conf. Ser.*, 2008, 97, p. 012005

[20] YAMASAKI, H., MAWATARI, Y., NAKAGAWA, Y. and YAMADA, H. Nondestructive, inductive measurement of critical current densities of superconducting films in magnetic fields. *IEEE Trans. Appl. Supercond.*, 2003, 13, p. 3718

[21] OHKI, K., YAMASAKI, H., DEVELOS-BAGARINAO, K. and NAKAGAWA, Y. Enhanced random pinning with oxygen annealing in YBCO films prepared by large-area pulsed laser deposition. *Supercond. Sci. Technol.*, 2008, 21, p. 045004

[22] SIMON, RW., HAMMOND, RB., BERKOWITZ, SJ. and WILLEMSEN, BA. Superconducting microwave filter systems for cellular telephone base stations. *Proceedings of the IEEE*, 2004, 92, p. 1585

[23] CHEGGOUR, N., EKIN, J.W., CLICKNER, CC., VEREBELYI, DT., THIEME, .LH., FEENSTRA, R., GOYAL, A. and PARANTHAMAN, M. Transverse compressive stress effect in Y-Ba-Cu-O coatings on biaxially textured Ni and Ni-W substrates. *IEEE Trans. Appl. Supercond.*, 2003, 13, p. 3530

[24] NAKAGAWA, Y., MAWATARI, Y., YAMASAKI, H., MURUGESAN, M. and DEVELOS-BAGARINAO, K. Angular hysteresis in the critical current density of laser-patterned $REBa_2Cu_3O_y$ films. *IEEE Trans. Appl. Supercond.*, 2007, 17, p. 3597

[25] KAIHO, K., OHARA, T., KOYAMA, K. and NAMBA, T. Calculation of Magnetic Field Distribution of Solenoid Coil by Computer, *J. IEE Japan*, 1977, 97, p. 237 (in Japanese)

[26] TONG, H. M., SAENGER, K. L. and SU, G. W., Thickness-direction thermal expansion of polyimide films, *Polymer Eng. Sci.*, 1993, 33, p. 1502

[27] MAWATARI Y. and CLEM, JR. Analytical model of the response of a superconducting film to line currents, Phys. Rev. B, 2006, 74, p. 144523

[28] TANAKA H., MAWATARI Y. and YAMASAKI H., Influence of coil configuration to measurement of J_c in superconducting thin film using third-harmonic voltage, *Abstracts of CSSJ Conference*, 2004, 71, p. 110 (in Japanese)

[29] NADAMI, T., OTABE, ES., KIUCHI, M. and MATSUSHITA, T. Dependence of induced third harmonic voltage on width of superconducting coated conductor, *Physica C*, 2004, 412–414, p. 1011

[30] GRIMALDI, G., BAUER, M. and KINDER, H. Continuous reel-to-reel measurement of critical currents of coated conductors. *Appl. Phys. Lett*., 2001, 79, p. 4390

[31] GRIMALDI, G., BAUER, M., KINDER, H., PRUSSEIT, W., GAMBARDELLA, Y. and PACE S. Magnetic imaging of YBCO coated conductors by Hall probes. *Physica C*, 2002, 372–376, p. 1009

[32] CLAASSEN, JH. Measurement of the Critical Current and Flux Creep Parameters in Thin Superconducting Films Using the Single Coil Technique. *IEEE Trans. Appl. Supercond.*, 1997, 7, p. 1463

[33] SUMIYOSHI, F., MATSUYAMA, M., NODA, M., MATSUSHITA, T., FUNAKI, K., IWAKUMA, M. and YAMAFUJI, K. Anomalous Magnetic Behavior due to Reversible Fluxoid Motion in Superconducting Multifilamentary Wires with Very Fine Filaments. *Jpn. J. Appl. Phys.*, 1986, 25, p. L148

[34] MATSUSHITA, T., OTABE, ES. and NI, B. Effect of reversible fluxoid motion on AC susceptibility of high temperature superconductors. *Physica C*, 1991, 182, p. 95

[35] YOSHIDA, T., SHIBATA, M., KIUCHI, M., OTABE, ES., MATSUSHITA, T., FUTAMURA, M., KONISHI, H., MIYATA, S., IBI, A., YAMADA, Y. AND SHIOHARA, Y. Evaluation of film thickness dependency of the reversible fluxoid motion in the third harmonic voltage method. Physica C, 2007, 463-465, p.692

[36] KIUCHI, M., YAMATO H. and MATSUSHITA, T. Longitudinal elastic correlation length of flux lines along the c-axis in superconducting Bi-2212 single crystal. *Physica C*, 1996, 269, p. 242

[37] KIM, SB. The defect detection in HTS films on third-harmonic voltage method using various inductive coils. *Physica C*, 2007, 463–465, p. 702

[38] IEC 61788-3, *Superconductivity – Part 3: Critical current measurement – DC critical current of Ag- and/or Ag alloy-sheathed Bi-2212 and Bi-2223 oxide superconductors*

[39] HUSE, DA., FISHER, MPA. and FISHER, DS. Are superconductors really superconducting? *Nature*, 1992, 358, p. 553

[40] YAMASAKI, H., MAWATARI, Y., NAKAGAWA, Y. and YAMADA, H. Evaluation of uncertainty in the inductive measurement of critical current densities of superconducting films using third-harmonic voltages, *Cryogenics*, 2012, 52, p. 544

[41] NAKAO, K., HIRABAYASHI, I. and TAJIMA, S. Application of an inductive technique to the characterization of superconducting thin films based on power law *I-V* relations. *Physica C*, 2005, 426-431, p. 1127

IEC 61788-17

Edition 2.0 2021-04

INTERNATIONAL STANDARD

colour inside

Superconductivity –
Part 17: Electronic characteristic measurements – Local critical current density and its distribution in large-area superconducting films

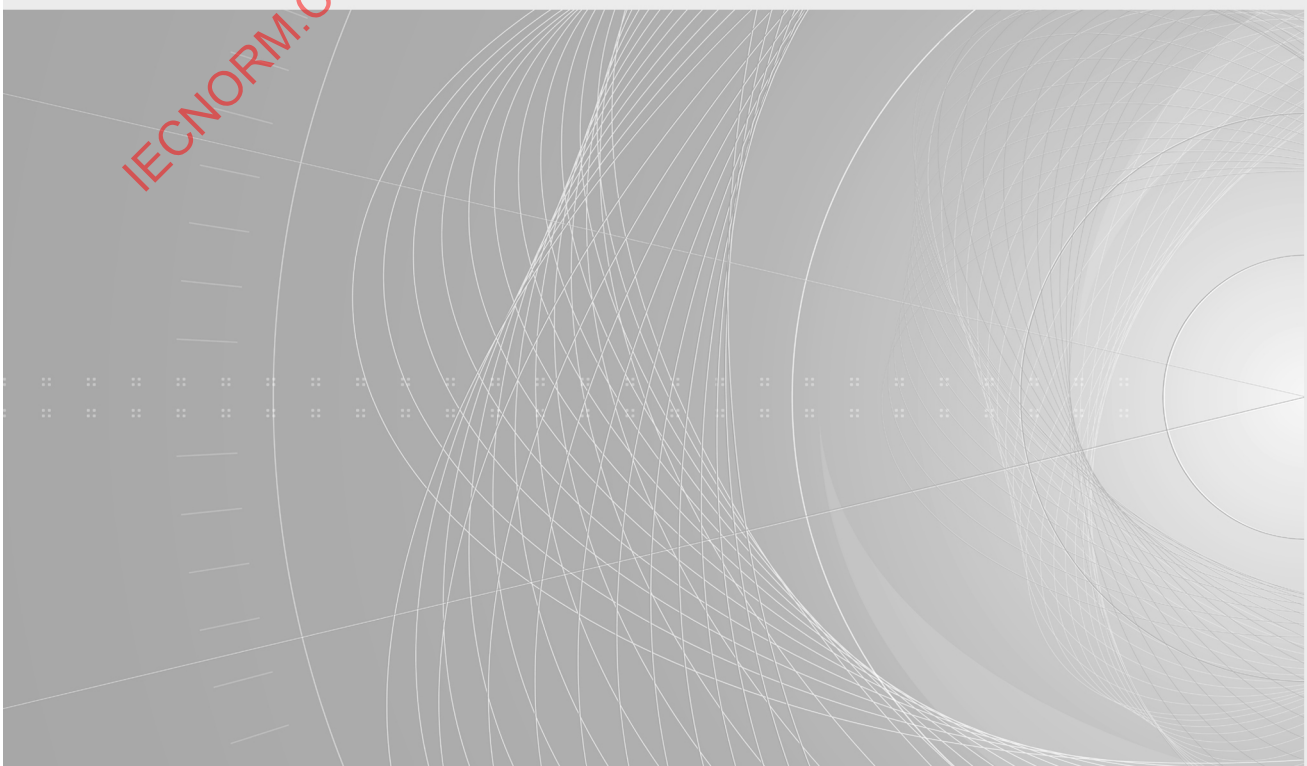

IEC 61788-17:2021-04(en)

CONTENTS

INTERNATIONAL ELECTROTECHNICAL COMMISSION

_____

SUPERCONDUCTIVITY –

Part 17: Electronic characteristic measurements – Local critical current density and its distribution in large-area superconducting films

FOREWORD

1) The International Electrotechnical Commission (IEC) is a worldwide organization for standardization comprising all national electrotechnical committees (IEC National Committees). The object of IEC is to promote international co-operation on all questions concerning standardization in the electrical and electronic fields. To this end and in addition to other activities, IEC publishes International Standards, Technical Specifications, Technical Reports, Publicly Available Specifications (PAS) and Guides (hereafter referred to as "IEC Publication(s)"). Their preparation is entrusted to technical committees; any IEC National Committee interested in the subject dealt with may participate in this preparatory work. International, governmental and non-governmental organizations liaising with the IEC also participate in this preparation. IEC collaborates closely with the International Organization for Standardization (ISO) in accordance with conditions determined by agreement between the two organizations.
2) The formal decisions or agreements of IEC on technical matters express, as nearly as possible, an international consensus of opinion on the relevant subjects since each technical committee has representation from all interested IEC National Committees.
3) IEC Publications have the form of recommendations for international use and are accepted by IEC National Committees in that sense. While all reasonable efforts are made to ensure that the technical content of IEC Publications is accurate, IEC cannot be held responsible for the way in which they are used or for any misinterpretation by any end user.
4) In order to promote international uniformity, IEC National Committees undertake to apply IEC Publications transparently to the maximum extent possible in their national and regional publications. Any divergence between any IEC Publication and the corresponding national or regional publication shall be clearly indicated in the latter.
5) IEC itself does not provide any attestation of conformity. Independent certification bodies provide conformity assessment services and, in some areas, access to IEC marks of conformity. IEC is not responsible for any services carried out by independent certification bodies.
6) All users should ensure that they have the latest edition of this publication.
7) No liability shall attach to IEC or its directors, employees, servants or agents including individual experts and members of its technical committees and IEC National Committees for any personal injury, property damage or other damage of any nature whatsoever, whether direct or indirect, or for costs (including legal fees) and expenses arising out of the publication, use of, or reliance upon, this IEC Publication or any other IEC Publications.
8) Attention is drawn to the Normative references cited in this publication. Use of the referenced publications is indispensable for the correct application of this publication.
9) Attention is drawn to the possibility that some of the elements of this IEC Publication may be the subject of patent rights. IEC shall not be held responsible for identifying any or all such patent rights.

IEC 61788-17 has been prepared by IEC technical committee 90: Superconductivity. It is an International Standard.

This second edition cancels and replaces the first edition published in 2013. This edition constitutes a technical revision.

This edition includes the following a significant technical change with respect to the previous edition:

a) A simple method to calculate theoretical coil coefficient k is described in 6.2.1.

The text of this International Standard is based on the following documents:

FDIS	Report on voting
90/462/FDIS	90/464/RVD

Full information on the voting for the approval of this International Standard can be found in the report on voting indicated in the above table.

The language used for the development of this International Standard is English.

This document was drafted in accordance with ISO/IEC Directives, Part 2, and developed in accordance with ISO/IEC Directives, Part 1 and ISO/IEC Directives, IEC Supplement, available at www.iec.ch/members_experts/refdocs. The main document types developed by IEC are described in greater detail at www.iec.ch/standardsdev/publications.

A list of all the parts of the IEC 61788 series, published under the general title *Superconductivity*, can be found on the IEC website.

The committee has decided that the contents of this document will remain unchanged until the stability date indicated on the IEC website under "http://webstore.iec.ch" in the data related to the specific document. At this date, the document will be

- reconfirmed,
- withdrawn,
- replaced by a revised edition, or
- amended.

IMPORTANT – The 'colour inside' logo on the cover page of this publication indicates that it contains colours which are considered to be useful for the correct understanding of its contents. Users should therefore print this document using a colour printer.

INTRODUCTION

Over thirty years after their discovery in 1986, high-temperature superconductors are now finding their way into products and technologies that will revolutionize information transmission, transportation, and energy. Among them, high-temperature superconducting (HTS) microwave filters, which exploit the extremely low surface resistance of superconductors, have already been commercialized. They have two major advantages over conventional non-superconducting filters, namely: low insertion loss (low noise characteristics) and high frequency selectivity (sharp cut) [1][1]. These advantages enable a reduced number of base stations, improved speech quality, more efficient use of frequency bandwidths, and reduced unnecessary radio wave noise.

Large-area superconducting thin films have been developed for use in microwave devices [2]. They are also considered for use in emerging superconducting power devices, such as resistive-type superconducting fault-current limiters (SFCLs) [3] [4] [5], superconducting fault detectors used for superconductor-triggered fault current limiters [6] [7] and persistent-current switches used for persistent-current HTS magnets [8] [9]. The critical current density J_c is one of the key parameters that describe the quality of large-area HTS films. Nondestructive, AC inductive methods are widely used to measure J_c and its distribution for large-area HTS films [10] [11] [12] [13], among which the method utilizing third-harmonic voltages $U_3\cos(3\omega t + \theta)$ is the most popular [10] [11], where ω, t and θ denote the angular frequency, time, and initial phase, respectively. However, these conventional methods are not accurate because they have not considered the electric-field E criterion of the J_c measurement [14] [15] and sometimes use an inappropriate criterion to determine the threshold current I_{th} from which J_c is calculated [16]. A conventional method can obtain J_c values that differ from the accurate values by 10 % to 20 % [15]. It is thus important to establish standard test methods to precisely measure the local critical current density and its distribution, to which all involved in the HTS filter industry can refer for quality control of the HTS films. Background knowledge on the inductive J_c measurements of HTS thin films is summarized in Annex A.

In these inductive methods, AC magnetic fields are generated with AC currents $I_0\cos\omega t$ in a small coil mounted just above the film, and J_c is calculated from the threshold coil current I_{th}, at which full penetration of the magnetic field to the film is achieved [17]. For the inductive method using third-harmonic voltages U_3, U_3 is measured as a function of I_0, and the I_{th} is determined as the coil current I_0 at which U_3 starts to emerge. The induced electric fields E in the superconducting film at $I_0 = I_{th}$, which are proportional to the frequency f of the AC current, can be estimated by a simple Bean model [14]. A standard method has been proposed to precisely measure J_c with an electric-field criterion by detecting U_3 and obtaining the n-value (index of the power-law E-J characteristics) by measuring I_{th} precisely at various frequencies [14] [15] [18] [19]. This method not only obtains precise J_c values, but also facilitates the detection of degraded parts in inhomogeneous specimens, because the decline of n-value is more noticeable than the decrease of J_c in such parts [15]. It is noted that this standard method is excellent for assessing homogeneity in large-area HTS films, although the relevant parameter for designing microwave devices is not J_c, but the surface resistance. For application of large-area superconducting thin films to SFCLs, knowledge on J_c distribution is vital, because J_c distribution significantly affects quench distribution in SFCLs during faults.

The International Electrotechnical Commission (IEC) draws attention to the fact that it is claimed that compliance with this document may involve the use of a patent. IEC takes no position concerning the evidence, validity, and scope of this patent right.

[1] Numbers in square brackets refer to the Bibliography.

The holder of this patent right has assured IEC that s/he is willing to negotiate licences under reasonable and non-discriminatory terms and conditions with applicants throughout the world. In this respect, the statement of the holder of this patent right is registered with IEC. Information may be obtained from the patent database available at http://patents.iec.ch.

Attention is drawn to the possibility that some of the elements of this document may be the subject of patent rights other than those in the patent database. IEC shall not be held responsible for identifying any or all such patent rights.

SUPERCONDUCTIVITY –

Part 17: Electronic characteristic measurements – Local critical current density and its distribution in large-area superconducting films

1 Scope

This part of IEC 61788 specifies the measurements of the local critical current density (J_c) and its distribution in large-area high-temperature superconducting (HTS) films by an inductive method using third-harmonic voltages. The most important consideration for precise measurements is to determine J_c at liquid nitrogen temperatures by an electric-field criterion and obtain current-voltage characteristics from its frequency dependence. Although it is possible to measure J_c in applied DC magnetic fields [20] [21], the scope of this document is limited to the measurement without DC magnetic fields.

This technique intrinsically measures the critical sheet current that is the product of J_c and the film thickness d. The range and measurement resolution for $J_c d$ of HTS films are as follows.

– $J_c d$: from 200 A/m to 32 kA/m (based on results, not limitation).

– Measurement resolution: 100 A/m (based on results, not limitation).

2 Normative references

The following documents are referred to in the text in such a way that some or all of their content constitutes requirements of this document. For dated references, only the edition cited applies. For undated references, the latest edition of the referenced document (including any amendments) applies.

IEC 60050-815, *International Electrotechnical Vocabulary – Part 815: Superconductivity* (available at <http://www.electropedia.org>)

3 Terms and definitions

For the purposes of this document, the terms and definitions given in IEC 60050-815 apply, some of which are repeated here for convenience.

ISO and IEC maintain terminological databases for use in standardization at the following addresses:

- IEC Electropedia: available at http://www.electropedia.org/
- ISO Online browsing platform: available at http://www.iso.org/obp

3.1
critical current
I_c
maximum direct current that can be regarded as flowing without resistance practically

Note 1 to entry: I_c is a function of magnetic field strength, temperature and strain.

[SOURCE: IEC 60050-815:2015, 815-12-01]

3.2
critical current criterion
I_c criterion
criterion to determine the critical current, I_c, based on the electric field strength, E, or the resistivity, ρ

Note 1 to entry: E = 10 µV/m or E = 100 µV/m is often used as electric field criterion, and $\rho = 10^{-14}$ Ω · m or $\rho = 10^{-13}$ Ω · m is often used as resistivity criterion.

[SOURCE: IEC 60050-815:2015, 815-12-02]

3.3
critical current density
J_c
electric current density at the critical current using either the cross-section of the whole conductor (overall) or of the non-stabilizer part of the conductor if there is a stabilizer

Note 1 to entry: The overall current density is called engineering current density (symbol: J_e).

[SOURCE: IEC 60050-815:2015, 815-12-03]

3.4
transport critical current density
J_{ct}
critical current density obtained by a resistivity or a voltage measurement

[SOURCE: IEC 60050-815:2015, 815-12-04]

3.5
***n*-value**
<superconductor> exponent obtained in a specific range of electric field strength or resistivity when the voltage/current U (I) curve is approximated by the equation $U \propto I^n$

[SOURCE: IEC 60050-815:2015, 815-12-10]

4 Requirements

The critical current density J_c is one of the most fundamental parameters that describe the quality of large-area HTS films. In this document, J_c and its distribution are measured non-destructively via an inductive method by detecting third-harmonic voltages $U_3\cos(3\omega t + \theta)$. A small coil, which is used both to generate AC magnetic fields and detect third-harmonic voltages, is mounted just above the HTS film and used to scan the measuring area. To measure J_c precisely with an electric-field criterion, the threshold coil currents I_{th}, at which U_3 starts to emerge, are measured repeatedly at different frequencies and the E-J characteristics are determined from their frequency dependencies.

The target relative combined standard uncertainty in the method used to determine the absolute value of J_c is less than 10 %. However, the target uncertainty is less than 5 % for the purpose of evaluating the homogeneity of J_c distribution in large-area superconducting thin films.

5 Apparatus

5.1 Measurement equipment

Figure 1 shows a schematic diagram of a typical electric circuit used for the third-harmonic voltage measurements. This circuit is comprised of a signal generator, power amplifier, digital multimeter (DMM) to measure the coil current, band-ejection filter to reduce the fundamental wave signals and lock-in amplifier to measure the third-harmonic signals. It involves the single-coil approach in which the coil is used to generate an AC magnetic field and detect the inductive voltage. This method can also be applied to double-sided superconducting thin films with no obstacles. In the methods proposed here, however, there is an additional system to reduce harmonic noise voltages generated from the signal generator and the power amplifier [14]. In an example of Figure 1, a cancel coil of specification being the same as the sample coil is used for cancelling. The sample coil is mounted just above the superconducting film, and a superconducting film with a $J_c d$ sufficiently larger than that of the sample film is placed below the cancel coil to adjust its inductance to that of the sample coil. Note that the inductance of the sample coil decreases by 20 % to 30 % due to the superconducting shielding current when it is mounted on a superconducting film. Both coils and superconducting films are immersed in liquid nitrogen (a broken line in Figure 1). Other optional measurement systems are described in Annex B.

NOTE In this circuit, coil currents of about 0,1 A (RMS) and power source voltages of > 6 V (RMS) are needed to measure the superconducting film of $J_c d \approx 10$ kA/m while using coil 1 or 2 of Table 2. A precision power amplifier with sufficiently high power is used to supply such large currents and voltages.

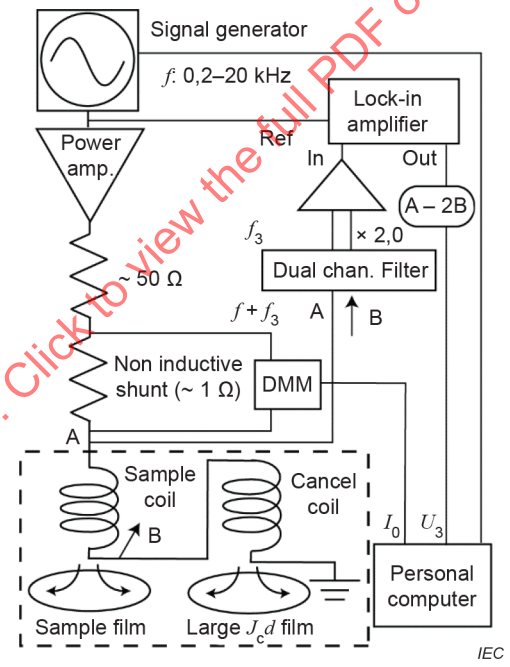

NOTE The broken line surrounds elements immersed in liquid nitrogen.

Figure 1 – Diagram for an electric circuit used for inductive J_c measurement of HTS films

5.2 Components for inductive measurements

5.2.1 Coils

Currently available large-area HTS films are deposited on areas as large as about 25 cm in diameter, while films about 5 cm in diameter are commercially used to prepare microwave filters [22]. Larger $YBa_2Cu_3O_7$ (YBCO) films, about 10 cm in diameter and 2,7 cm × 20 cm, were used to fabricate fault current limiter modules [3] [4] [5]. For the J_c measurements of such films, the appropriate outer diameter of the sample coils ranges from 2 mm to 5 mm. The requirement for the sample coil is to generate as high a magnetic field as possible at the upper surface of the superconducting film, for which flat coil geometry is suitable. Typical specifications are as follows.

a) Inner winding diameter D_1: 0,9 mm, outer diameter D_2: 4,2 mm, height h: 1,0 mm, 400 turns of a 50 µm diameter copper wire.

b) D_1: 0,8 mm, D_2: 2,2 mm, h: 1,0 mm, 200 turns of a 50 µm diameter copper wire.

5.2.2 Spacer film

Typically, a polyimide film with a thickness of 50 µm to 125 µm is used to protect the HTS films. The coil has generally some protection layer below the coil winding, which also insulates the thin film from Joule heat in the coil. The typical thickness is 100 µm to 150 µm, and the coil-to-film distance Z_1 is kept to be 200 µm.

5.2.3 Mechanism for the set-up of the coil

To maintain a prescribed value for the spacing Z_1 between the bottom of the coil winding and the film surface, the sample coil should be pressed to the film with sufficient pressure, typically exceeding about 0,2 MPa [18]. Techniques to achieve this are to use a weight or spring, as shown in Figure 2. The system schematically shown in the figure left is used to scan a wide area of the film. Before the U_3 measurement the coil is initially raised up to some distance, moved laterally to the target position, and then lowered down and pressed to the film. An appropriate pressure should be determined so that too high pressure does not damage the bobbin, coil, HTS thin film or the substrate. It is reported that the YBCO deposited on biaxially-textured pure Ni substrate was degraded by transverse compressive stress of about 20 MPa [23].

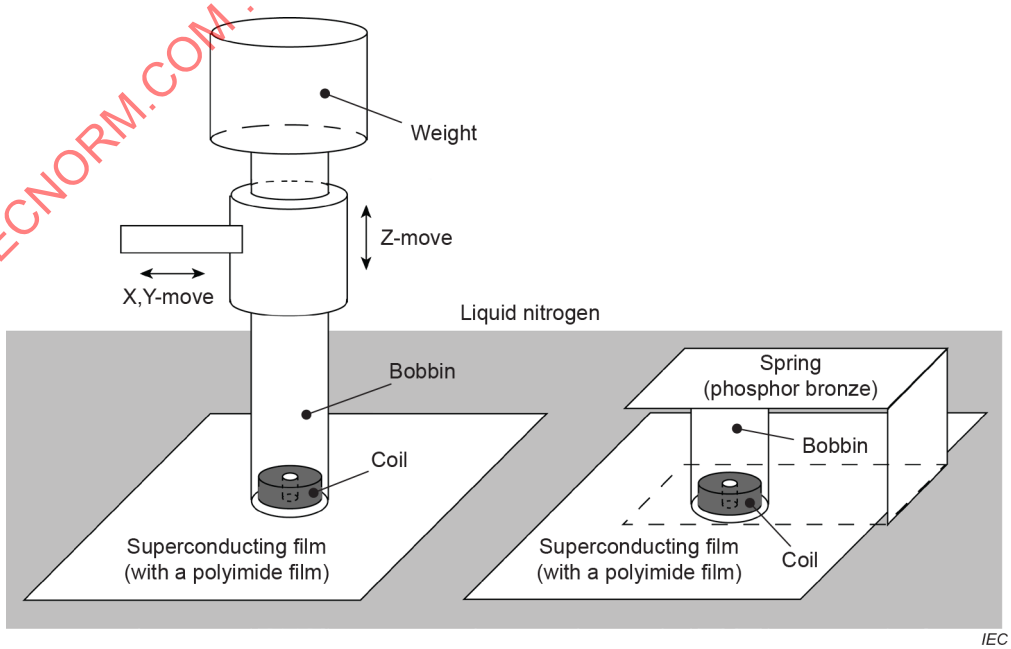

Figure 2 – Illustration showing techniques to press the sample coil to HTS films

5.2.4 Calibration wafer

A calibration wafer is used to determine the experimental coil coefficient k' described in Clause 6. It is made by using a homogeneous large-area (typically about 5 cm diameter) YBCO thin film. It consists of bridges for transport measurement and an inductive measurement area (Figure 3). Typical dimensions of the transport bridges are 20 µm to 70 µm wide and 1 mm to 2 mm long, which were prepared either by UV photolithography technique or by laser etching [24]. In the transport bridge area shown in Figure 3, a transport current can be passed from current terminal 1 to another current terminal 3 through the bridge "a". In this case, terminals 2 and 12 are used as voltage terminals. Similarly, a transport current can be passed from current terminal 1 to another current terminal (5, 7, 9 or 11) through the bridge "b", "c", "d" or "e". In this case, terminals 4, 6, 8 or 10, and 12 are used as voltage terminals.

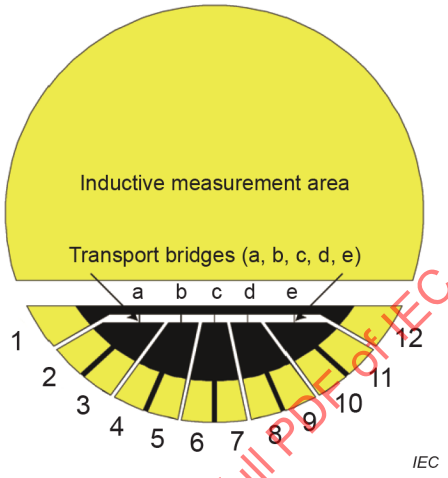

Figure 3 – Example of a calibration wafer used to determine the coil coefficient

6 Measurement procedure

6.1 General

The procedures used to determine the experimental coil coefficient k' and measure the J_c of the films under test are described as follows, with the meaning of k' expressed in Clause A.5.

6.2 Determination of the experimental coil coefficient

6.2.1 Calculation of the theoretical coil coefficient k

Calculate the theoretical coil coefficient $k = J_c d/I_{th}$ from

$$k = F_m, \tag{1}$$

where F_m is the maximum of $F(r)$ that is a function of r, the distance from the central axis of the coil whose inner diameter is D_1, outer diameter is D_2 and height is h (Figure 4). The coil-factor function $F(r) = -2H_r(r, t)/I_0 \cos\omega t = 2H_0/I_0$ is obtained by

$$F(r) = \frac{N}{2\pi S}\int_{R_1}^{R_2} dr' \int_0^{2\pi} d\theta \int_{Z_1}^{Z_2} dz \frac{r' z \cos\theta}{(z^2 + r^2 + r'^2 - 2rr'\cos\theta)^{3/2}}, \tag{2}$$

where $H_r(r, t)$ is the radial component of the magnetic field generated by the sample coil at a upper surface of the superconducting film, N is the number of turns in the sample coil, $R_1 = D_1/2$ is the inner radius, $R_2 = D_2/2$ is the outer radius of the coil, $S = (R_2 - R_1)h$ is the cross-sectional area, Z_1 is the coil-to-film distance, and $Z_2 = Z_1 + h$ [17]. The explanation of Equations (1) and (2) is given in Clause A.3.

A simple method to obtain k is as follows.

a) Calculate the magnetic-field amplitude $H_0(r) = H_r(r, t = 0)$ as a function of r at a position below the coil with a distance Z_1 when a current of I_0 = 1 mA is passed in the sample coil (Figure 5).

b) Obtain the (local) maximum value of $H_0(r)$ when r is changed near $r \approx (R_1 + R_2)/2$.

c) The maximum value of $H_0(r)$ should have a unit of A/m, then the doubled value divided by I_0 (= 1 mA) becomes k (unit: 1/mm). Note that the magnetic field arising from the image coil (i.e. from the shielding current flowing in the superconducting film) cancels out the perpendicular component H_z, and the parallel component H_r doubles. The image coil and its magnetic field generation are shown by the broken lines in Figure 5.

d) For the calculation of coil magnetic fields, a free web site may be used; for example, http://www.sc.kyushu-u.ac.jp/~kajikawa/javascript/field_and_potential-e.html
(the calculation of this site is based on a paper entitled "Calculation of Magnetic Field Distribution of Solenoid Coil by Computer" [25].[2]

Some examples of the theoretical coil coefficient k for typical sample coils are shown in Table 1 with the specifications.

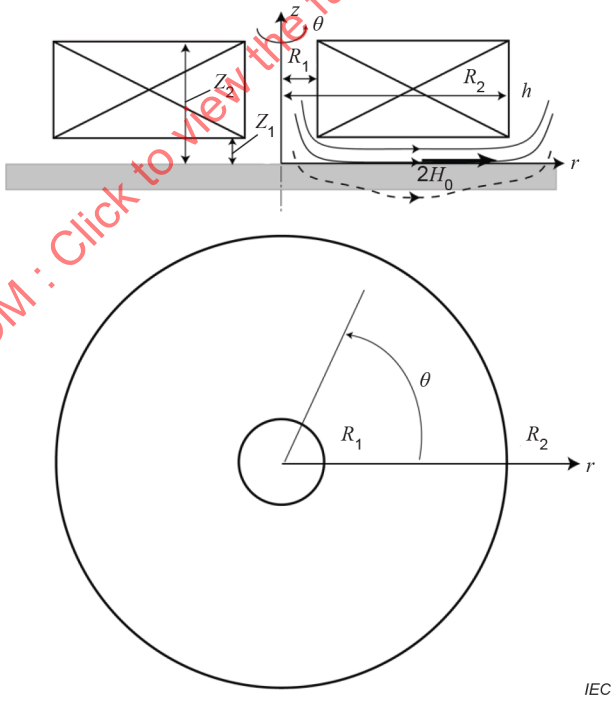

Figure 4 – Illustration of the sample coil and the magnetic field during measurement

2 This information is given for the convenience of users of this document and does not constitute an endorsement by IEC.

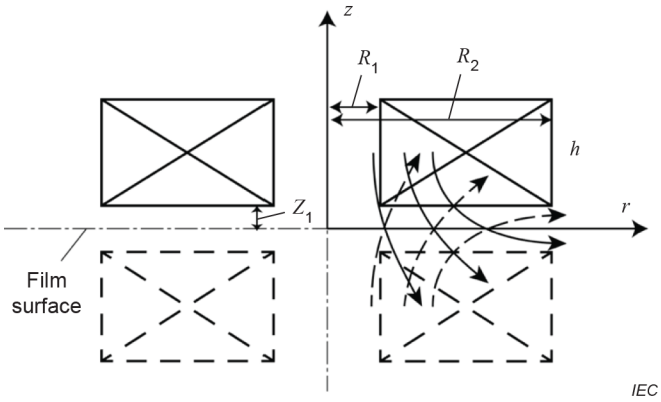

NOTE The image coil and its magnetic field generation are shown by the broken line.

Figure 5 – Illustration of the sample coil and its magnetic field generation

Table 1 – Specifications and theoretical coil coefficients k of sample coils

	D_1 mm	D_2 mm	h mm	Turns	k 1/mm	r at $F(r) = F_m$ mm
A1	0,8	2,2	1,0	200	62,9	0,74
A2	0,9	2,9	1,0	300	92,2	0,95
A3	1,0	3,6	1,0	400	117,4	1,15
A4	1,0	4,3	1,0	500	135,2	1,35
A5	1,0	4,9	1,0	600	151,5	1,52
A6	1,0	3,6	1,5	600	136,0	1,17
B1	1,0	4,3	1,0	150	34,4	1,35
B2	1,0	5,4	1,0	200	41,9	1,67
B3	1,0	6,5	1,0	250	47,9	1,98
B4	1,0	7,6	1,0	300	52,6	2,31
B5	1,5	5,4	1,5	300	51,5	1,68
Coils A1 to A6 are made of 50-μm-diameter copper wires (coil-to-film distance Z_1 = 0,2 mm), and coils B1 to B5 are made of 100-μm-diameter copper wires (coil-to-film distance Z_1 = 0,33 mm).						

6.2.2 Transport measurements of bridges in the calibration wafer

a) Measure the E-J characteristics of the transport bridges of the calibration wafer by a four-probe method, and obtain the power-law E-J characteristics,

$$E_t = A_{0t} \times J^n. \quad (3)$$

b) Repeat the measurement for at least three different bridges. Three sets of data (n = 20,5 to 23,8) measured for three bridges are shown in the upper (high-E) part of Figure 6.

6.2.3 U_3 measurements of the calibration wafer

a) Measure U_3 in the inductive measurement area of the calibration wafer as a function of the coil current with three or four frequencies, and obtain the experimental I_{th} using a constant-inductance criterion; namely, $U_3/fI_{th} = 2\pi L_c$. The criterion L_c should be as small as possible within the range with sufficiently large signal-to-noise (S/N) ratios, in order to use the simple Equation (4) for the electric-field calculation (7.1 c) and Clause C.2).

b) Repeat the measurement for at least three different points of the film.

6.2.4 Calculation of the E-J characteristics from frequency-dependent I_{th} data

a) Calculate J_{c0} (= kI_{th}/d) and the average E induced in the superconducting film at the full penetration threshold (when $J_c = J_{c0}$) by

$$E_{\text{avg-}U_3} \approx 2{,}04\mu_0 fd^2 J_c = 2{,}04\mu_0 kfdI_{th}\,, \tag{4}$$

from the obtained I_{th} at each frequency using the theoretical coefficient k calculated in 6.2.1. The derivation of Equation (4) is described in Clause A.4.

b) Obtain the E-J characteristics, and the electric fields E_i induced in the superconducting film can be approximated as

$$E_i = A_{0i} \times J^n\,, \tag{5}$$

from the relation between $E_{\text{avg-}U_3}$ and J_{c0}, and plot them in the same figure where the transport E-J characteristics data were plotted. Broken lines in Figure 6 show three sets of data measured at different points of the film. Transport data and U_3 inductive data do not yet match at this stage.

6.2.5 Determination of the k' from J_{ct} and J_{c0} values for an appropriate E

a) Choose an appropriate electric field that is within (or near to) both the transport E-J curves and the inductive E-J curves, such as 200 μV/m in Figure 6.

b) At this electric field, calculate both the transport critical current densities J_{ct} and the inductive J_{c0} values from Equation (3) and Equation (5), respectively.

c) Determine the experimental coil coefficient k' by $k' = (J_{ct}/J_{c0})k$, where J_{ct} and J_{c0} indicate the average values of obtained J_{ct} and J_{c0} values, respectively. If the J_c (= $k'I_{th}/d$) values are plotted against $E_{\text{avg-}U_3} = 2{,}04\mu_0 kfdI_{th}$, the E-J characteristics from the U_3 measurement match the transport data well (Figure 6).

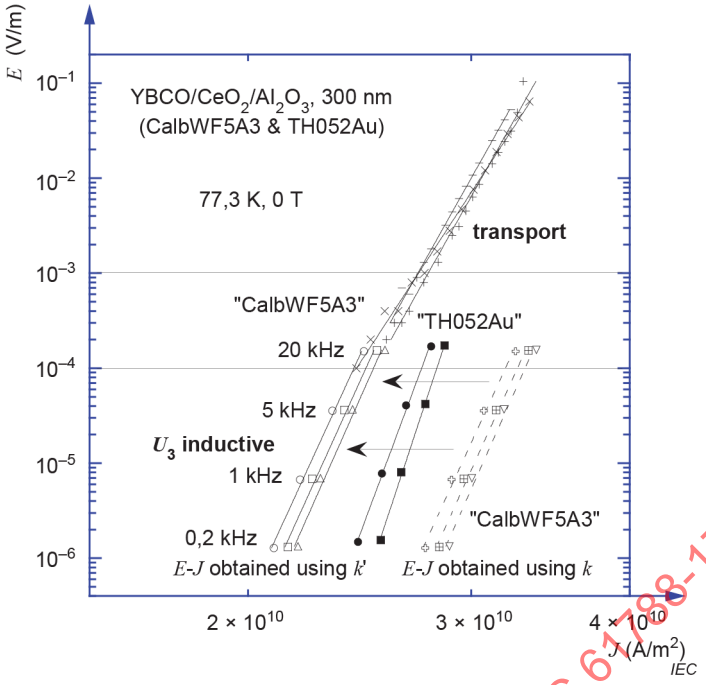

NOTE Broken lines show three sets of data measured at different points of the film.

Figure 6 – E-J characteristics measured by a transport method and the U_3 inductive method

6.3 Measurement of J_c in sample films

a) Measure U_3 with two, three or four frequencies in sample films, and obtain I_{th} with the same criterion L_c as used in 6.2.3.

b) Use the obtained experimental coil coefficient k' to calculate J_c (= $k'I_{th}/d$) at each frequency, and obtain the relation between J_c and $E_{avg\text{-}U_3}$ (= $2{,}04\mu_0 kfdI_{th}$) using k because of the underestimation as mentioned in 7.1 c). An example of the E-J characteristics is also shown in Figure 6, measured for a sample film (TH052Au, solid symbols) with n-values (36,0 and 40,4) exceeding those of the calibration wafer (n = 28,0 to 28,6).

c) From the obtained E-J characteristics, calculate the J_c value with an appropriate electric-field criterion, such as E_c = 100 µV/m.

d) Measurement with three or four frequencies is beneficial to check the validity of the measurement and sample by checking the power-law E-J characteristics. Measurement with two frequencies can be used for routine samples in the interests of time.

6.4 Measurement of J_c with only one frequency

As mentioned in Clause 1 and Clause 3, it is recommended to determine J_c with a constant electric-field criterion using a multi-frequency approach through procedures described in 6.2 and 6.3, because a supercurrent flowing in a superconductor is a function of electric field. However, one frequency measurement is sometimes desired for simplicity and inexpensiveness. In this case, the J_c values are determined with variable electric-field criteria as specified in the following procedures.

a) Calculate the theoretical coil coefficient k as described in 6.2.1.

b) Obtain the E-J characteristics of the transport bridges of the calibration wafer (Equation (3)) through the procedures of 6.2.2.

c) Measure U_3 in the inductive measurement area of the calibration wafer as a function of the coil current with one frequency, and obtain the experimental I_{th} using a constant-inductance criterion; namely, $U_3/fI_0 = 2\pi L_c$. The criterion L_c should be as small as possible within the range with sufficiently large S/N ratios, in order to use the simple Equation (4) in 6.2.4 for the electric-field calculation. Calculate J_{c0} (= kI_{th}/d) and the average E induced in the superconducting film at the full penetration threshold by Equation (4). Repeat the measurement for at least three different points of the film, and obtain average J_{c0} and $E_{avg\text{-}U_3}$

d) Using the transport E-J characteristics of Equation (3), calculate J_{ct} for the average $E_{avg\text{-}U_3}$ obtained in c).

e) Determine the experimental coil coefficient k' by $k' = (J_{ct}/J_{c0})k$.

f) Measure U_3 with the same frequency in sample films, and obtain I_{th} with the same criterion L_c as used in c). Calculate J_c (= $k'I_{th}/d$) using the obtained experimental coil coefficient k'. Calculate also $E_{avg\text{-}U_3}$ with Equation (4), and this value should be accompanied by each J_c value.

6.5 Examples of the theoretical and experimental coil coefficients

Some examples of the theoretical and experimental coil coefficients (k and k') for typical sample coils are shown in Table 2 with the specifications and recommended criteria for the I_{th} determination, $2\pi L_c = U_3/fI_0$. Note that the k' depends on the criterion L_c. Coils 1 and 2 are wound with a 50 µm diameter, polyurethane enamelled round copper winding wire, and coil 3 is wound with a 50 µm diameter, self-bonding polyurethane enamelled round copper winding wire. Measured resistances at 77,3 K and calculated self-inductances when a superconducting film is placed below the coil are also shown. The coil-to-film distance Z_1 is fixed at 0,2 mm. The images of coils 1 and 3 are shown in Figure 7, and the coil-factor functions $F(r)$ for the three coils show that the peak magnetic field occurs near the mean coil radius (Figure 8).

Table 2 – Specifications and coil coefficients of typical sample coils

	D_1 mm	D_2 mm	h mm	Turns	k 1/mm	k' 1/mm	U_3/fI_0 µΩ·s	R Ω	L mH
1	0,8	2,2	1,0	200	62,9	47,0	0,6	1,6	0,028
2	1,0	3,6	1,0	400	117,4	89,1	2	3,4	0,163
3	0,9	4,2	1,0	400	106,6	82,2	2	4,1	0,165

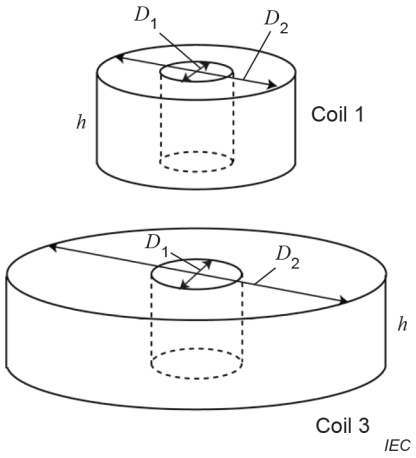

Figure 7 – Illustration of coils 1 and 3 in Table 2

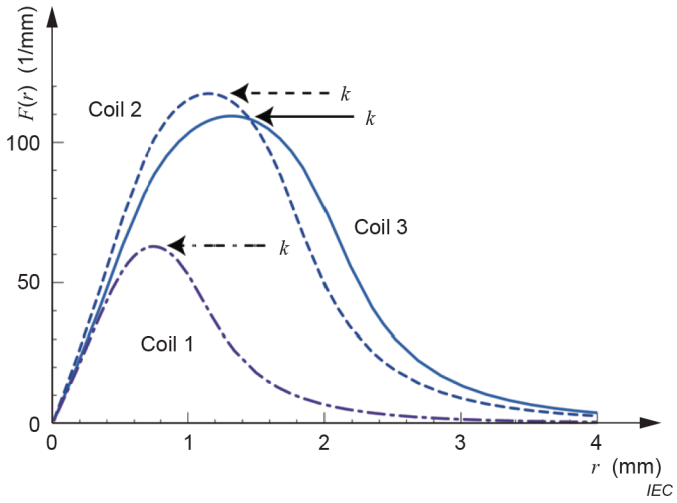

Figure 8 – The coil-factor function $F(r) = 2H_0/I_0$ calculated for the three coils

7 Uncertainty in the test method

7.1 Major sources of systematic effects that affect the U_3 measurement

The most significant systematic effect on the U_3 measurement is due to the deviation of the coil-to-film distance Z_1 from the prescribed value. Because the measured value $J_c d$ in this technique is directly proportional to the magnetic field at the upper surface of the superconducting film, the deviation of the spacing Z_1 directly affects the measurement. The key origins of the uncertainty are listed in a) to c) below.

a) Inadequate pressing of the coil to the film

As the measurement is performed in liquid nitrogen, the polyimide film placed above the HTS thin film becomes brittle and liquid nitrogen may enter the space between the polyimide and HTS films. Thus, sufficient pressure is needed to keep the polyimide film flat and avoid the deviation of Z_1. An experiment has shown that the required pressure is about 0,2 MPa [18]. Here it is to be noted that thermal contraction of polyimide films at the liquid nitrogen temperature is less than 0,008 × (300 − 77) ≈ 1,78 %, which leads to negligible values of 0,9 µm to 4,5 µm compared with the total coil-to-film distance (about 200 µm) [26].

b) Ice layer formed between the coil and polyimide film

The liquid nitrogen inevitably contains powder-like ice. If the sample coil is moved to scan the large-area HTS film area for an extended period, an ice layer is often formed between the polyimide film and the sample coil, which increases the coil-to-film distance Z_1 from the prescribed value. As shown later in 7.2, this effect reduces coil coefficients (k and k'), and the use of uncorrected k' results in an overestimate in J_c. Special care should be taken to keep the measurement environment as dry as possible. If the measurement system is set in an open (ambient) environment, the J_c values measured after an extended period of time become sometimes greater than those measured before, and the overestimation was as large as 6 % when measured after one hour. If the measurement system is set in almost closed environment and the ambient humidity is kept less than about 5 %, such effect of ice layers can be avoided. We can check this effect by confirming reproducibility. If the same J_c values are obtained after an extended period, it proves that there is negligible effect of ice layers. These two systematic effects (a) and b)) are not considered in the estimate of the uncertainty in the experimental coil coefficient k' in 7.3 and Clause C.1, because they can be eliminated by careful measurements.

c) Underestimation of the induced electric field E by a simple Bean model

The calculation of average induced electric fields $E_{\text{avg-}U_3}$ in the superconducting film via Equation (4) is sufficiently accurate provided the magnetic-field penetration below the bottom of the film can be neglected. However, considerable magnetic fields penetrate below the film when the experimental threshold current I_{th} is determined and detectable U_3 has emerged. It was pointed out that the rapid magnetic-field penetration below the film at $I_0 = I_{\text{th}}$ may cause a considerable increase of the induced electric field and that the E calculated by Equation (4) might be significantly underestimated [27]. However, several experimental results have shown that the relative standard uncertainty from this effect is usually less than 5 %. The detail is described in Clause C.2.

7.2 Effect of deviation from the prescribed value in the coil-to-film distance

Because the magnetic field arising from the coil depends on the coil-to-film distance Z_1, the coil coefficient also depends on Z_1. Figure 9 shows the Z_1 dependence of the theoretical coil coefficient k calculated from Equations (1) and (2). The theoretical coil coefficient k normalized by k_0 is plotted as the function of Z_1, where k_0 is the theoretical coil coefficient for Z_1 = 0,2 mm. Dimensions of coils 1, 2, and 3 are listed in Table 2. The relative effect of deviation on k of coil 3 is about 2,6 %, when Z_1 = 0,2 mm ± 0,02 mm. Provided the deviation of Z_1 is small (e.g. ≤ 20 %), the deviated experimental coil coefficient k' is proportional to k. Some experimental results that support this are described in Clause C.3. Therefore, use Figure 9 to estimate the systematic effect on k', if the deviated distance can be reasonably estimated.

The effect of the coil inclination to the superconducting film was theoretically investigated [28]. It was found that the theoretical coil coefficient k decreases approximately 7 % when the sample coil (D_1 = 1,0 mm, D_2 = 3,6 mm, h = 1 mm) is inclined 4 % and the distance between the coil and the superconducting thin film is increased.

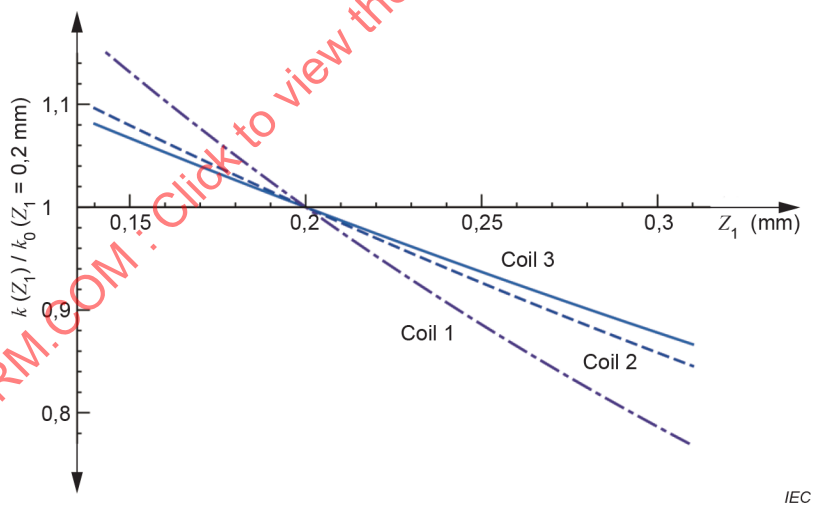

Figure 9 – The coil-to-film distance Z_1 dependence of the theoretical coil coefficient k

7.3 Uncertainty in the experimental coil coefficient and the obtained J_c

Since the proposed method uses a standard sample (the calibration wafer) to determine the experimental coil coefficient k' that directly affects the measured J_c values, the uncertainty in k' is one of the key factors affecting the uncertainty in the measurement, and the homogeneity of the large-area thin film used in the calibration wafer is an important source of such uncertainty. The experimental coil coefficient k' is calculated by $k' = (J_{ct}/J_{c0})k$ at an appropriate electric field, where J_{ct} is the critical current density measured by the transport method and $J_{c0} = kI_{th}/d$ measured by the inductive method (6.2.5). An example of the evaluation of the uncertainty in k' for the coil 3 (Table 2) is shown in Clause C.1. The result is $k' = (J_{ct}/J_{c0})k$ = {(2,587 8 × 10^{10} A/m^2)/(3,355 6 × 10^{10} A/m^2)} × 106,6 mm^{-1} = 82,2 mm^{-1} with the combined standard uncertainty in $u_c(k')$ = 2,4 mm^{-1} (2,93 %). It has been demonstrated that the uncertainty in the transport J_{ct} dominates the combined standard uncertainty in k'.

The uncertainty originating from the underestimation of $E_{\text{avg-}U_3}$ by a simple Bean model (Equation (4)) is evaluated in Clause C.2. The relative standard uncertainty (Type B) is evaluated to be u_B = 6,6/$\sqrt{3}$ % = 3,8 % for a typical specimen with n = 25. In contrast to these Type-B uncertainties, Type-A uncertainty in J_c, originating from the experimental uncertainty in the electric U_3 measurement, is much smaller, typically about 0,3 %, as shown in Clause C.4. The uncertainty in k' and that from the underestimation of $E_{\text{avg-}U_3}$ dominate the combined standard uncertainty in the absolute value of J_c, and the relative combined standard uncertainty was 4,7 % for a typical $DyBa_2Cu_3O_7$ (DyBCO) sample film (Clause C.5). This is well below the target value of 10 %. Note that for the purpose of evaluating the homogeneity of J_c distribution in large-area superconducting thin films, the uncertainty in k' does not contribute to the uncertainty in J_c distribution, provided the same sample coil is used. Therefore, the relative standard uncertainty should be less than the target uncertainty of 5 %.

7.4 Effects of the film edge

Figure 8 shows that substantial magnetic fields exist, even outside the coil area, which induce shielding currents in the superconducting film. Therefore, the coil needs to be apart from the film edge for the precise measurement. The original paper by Claassen *et al*. recommended that the outer diameter of the coil should be less than half of the film width to neglect the edge effect [10]. However, recent numerical calculation with the finite element method indicated that correct measurements can be made when the film width is as small as 6 mm for a coil with an outer diameter of 5 mm and for Z_1 = 0,2 mm [29]. The experimental results described in Clause C.6 have shown that precise measurements can be made for either of coils 2 or 3 (Table 2) when the outside of the coil is more than 0,3 mm apart from the film edge. With the uncertainty of 0,1 mm to 0,2 mm in the coil setting in mind, the outside of the coil should be more than 0,5 mm apart from the film edge when coils with an outer diameter of 2 mm to 5 mm are used.

7.5 Specimen protection

Moisture and water sometimes react with the Ba atoms in the YBCO film and cause the superconducting properties to deteriorate. If YBCO films are still used for some purpose after the measurement, they should be warmed up in a moisture-free environment, e.g. a vacuum or He gas to avoid degradation. Some protection measure can also be provided for the specimens. A thin organic coating, with thickness less than several micrometres, does not affect the measurements and can subsequently be removed; thus it can be used for protection.

8 Test report

8.1 Identification of test specimen

The test specimen shall be identified, if possible, by the following:

a) name of the manufacturer of the specimen;
b) classification;
c) lot number;
d) chemical composition of the thin film and substrate;
e) thickness and roughness of the thin film;
f) manufacturing process technique.

8.2 Report of J_c values

The J_c values shall be reported with the electric-field criterion, E_c. If possible, the n-values, the indices of the power-law E-J characteristics, shall be reported together. It is known that the measurement of n-values facilitates the detection of degraded segments within a large-area HTS film [15].

8.3 Report of test conditions

The following test conditions shall be reported:

a) temperature (atmospheric pressure, or the pressure of liquid nitrogen);
b) DC magnetic fields (if applied);
c) test frequencies;
d) possible effects of the ice layer;
e) specifications of the sample coil;
f) thickness of the spacer film.

Annex A
(informative)

Additional information relating to Clauses 1 to 8

A.1 Comments on other methods for measuring the local J_c of large-area HTS films

There are several AC inductive methods for the nondestructive measurement of local J_c of large-area superconducting thin films [10] [11] [12] [13] [17], in which some detect third-harmonic voltages $U_3\cos(3\omega t + \theta)$ [10] [11] [17] and others use only the fundamental voltage [12] [13]. In these inductive methods, AC magnetic fields are generated with AC currents $I_0\cos\omega t$ in a small coil mounted just above the film, and J_c is calculated from the threshold coil current I_{th}, at which full penetration of the AC magnetic field to the film is achieved [14]. When $I_0 < I_{th}$, the magnetic field below the film is completely shielded, and the superconducting film is regarded as a mirror image coil reflected through the upper surface of the film, carrying the same current but in the opposite direction. The response of the superconducting film to $I_0\cos\omega t$ is linear and no third-harmonic voltage is induced in the coil.

For the case of the U_3 inductive method, U_3 starts to emerge at $I_0 = I_{th}$, when the superconducting shielding current reaches the critical current and its response becomes nonlinear [17]. In the other methods that use only the fundamental voltage, to detect the breakdown of complete shielding when the critical current is reached, penetrated AC magnetic fields are detected by a pickup coil mounted just below the film [12] or a change of mutual inductance of two adjacent coils is measured [13]. In all these inductive J_c measurements, the scheme is common in that the AC magnetic field $2H_0\cos\omega t$ at the upper surface of the film is measured at the full penetration threshold. We obtain J_c because the amplitude of the full penetration field $2H_0$ equals $J_c d$ [17]. The electric field E induced in the superconductor can be calculated with the same Equation (4) [14], and a similar procedure to that described in Clause 6 can be used for the precise measurement.

Another inductive magnetic method using Hall probe arrays has been commercialized to measure local J_c of long coated conductors [30] [31]. In this method magnetic field profiles are measured in applied DC magnetic field, and the corresponding current distribution is calculated. This method can also be applied to rectangular large-area HTS films having widths less than several centimetres, and has better spatial resolution over AC inductive methods using small coils.

A.2 Requirements

As the third-harmonic voltages are proportional to the measuring frequency, higher frequencies are desirable to obtain a better S/N ratio. However, there is a limitation due to the frequency range of the measuring equipment (lock-in amplifier and/or filter) and to excessive signal voltages induced in the sample coil when a large $J_c d$ film is measured. It is recommended to use a frequency from 1 kHz to 20 kHz for a film with small $J_c d$ (≤ 1 kA/m), and a frequency from 0,2 kHz to 8 kHz for a film with large $J_c d$ (≥ 20 kA/m). Measurements over a wide frequency range are desirable to obtain the current-voltage characteristics in a wide electric-field range. For the general purpose of the J_c measurement, however, one order of frequency range is sufficient to obtain the n-value and measure J_c precisely.

In this document, the measurement temperature is limited to liquid nitrogen temperatures, namely 77,35 K at 1 013 hPa and 65,80 K at 200 hPa, because a refrigerant is needed to cool the sample coil that generates Joule heat. When measuring at variable temperatures in a gas atmosphere, further investigations are necessary.

The U_3 inductive method is applicable not only to large-area HTS films deposited on insulating substrates (sapphire, MgO, etc.), but also to coated conductors with metallic substrates. However, if the coated conductors have thick metallic protective layers (Ag or Cu) and their thickness exceeds about 10 µm, certain measures are needed to avoid the skin effect. One technique involves limiting measuring frequencies to a sufficiently low extent (e.g. about 8 kHz).

A.3 Theory of the third-harmonic voltage generation

Here we present the response of a superconducting film to a current-carrying coil mounted above the film (Figure A.1) [17]. A superconducting film of thickness d, infinitely extended in the xy plane, is situated at $-d < z < 0$, where the upper surface is at $z = 0$ in the xy plane and the lower surface is at $z = -d$. A drive coil is axially symmetric with respect to the z-axis, and the coil occupies the area of $R_1 < r < R_2$ and $Z_1 < z < Z_2$ in the cylindrical coordinate (r, θ, z). The coil consists of a wire of N turns, which carries a sinusoidal drive current $I_d(t) = I_0 \cos\omega t$ along the θ direction. Responding to the magnetic field produced by the coil, the shielding current flows in the superconducting film. The sheet current K_θ (i.e. the current density integrated over the thickness, $-d < z < 0$) in the superconducting film plays crucial roles in the response of the film, and $|K_\theta|$ cannot exceed its critical value, $J_c d$.

The response of the superconducting film is detected by measuring the voltage $U(t)$ induced in the coil, and $U(t)$ is generally expressed as the Fourier series,

$$U(t) = \sum_{n=1}^{\infty} U_n \cos(n\omega t + \theta_n) \,. \tag{A.1}$$

The fundamental voltage U_1 is primarily determined by the coil impedance. The even harmonics, U_n for even n, is generally much smaller than the odd harmonics, U_n for odd n. The third-harmonic voltage, U_3, is the key, because U_3 directly reflects the nonlinear response (i.e. information on $J_c d$) of the superconducting film.

The coil produces an axially symmetric magnetic field, and its radial component H_r at the upper surface of the superconducting film ($z = 0$) is obtained by

$$H_r(r,t) = -H_0 \cos\omega t = -(I_0/2) F(r) \cos\omega t \,. \tag{A.2}$$

The coil-factor function $F(r)$ is determined by the configuration of the coil as

$$F(r) = \frac{N}{2\pi S} \int_{R_1}^{R_2} \mathrm{d}r' \int_0^{2\pi} \mathrm{d}\theta \int_{Z_1}^{Z_2} \mathrm{d}z \frac{r' z \cos\theta}{(z^2 + r^2 + r'^2 - 2rr'\cos\theta)^{3/2}} \,, \tag{A.3}$$

where $S = (R_2 - R_1)(Z_2 - Z_1)$ is the cross-sectional area of the coil. The $F(r)$ generally has a maximum $F_m > 0$ at $r = r_m$ [where r_m is roughly close to $(R_1 + R_2)/2$], and $F(0) = F(\infty) = 0$.

When $0 < I_0 < I_{th}$, the magnetic field arising from the coil does not penetrate below the film ($z < -d$). In such cases, the magnetic field distribution above the film ($z > 0$) is simply obtained by the mirror-image technique. The magnetic field arising from the image coil (i.e. from the shielding current flowing in the superconducting film) cancels out the perpendicular component H_z, and the parallel component H_r doubles. The sheet current K_θ in the superconducting film is therefore obtained by $K_\theta(r, t) = 2H_r(r, t) = -I_0F(r)\cos\omega t$. Because of the linear response of the superconducting film for $0 < I_0 < I_{th}$, the voltage induced in the coil contains no harmonics.

Note that the amplitude of the sheet current density, $|K_\theta| = 2|H_r| = I_0F(r) \le I_0F_m$, cannot exceed the critical value, J_cd, when $0 < I_0 \le I_{th}$. The threshold current I_{th} is determined such that $|K_\theta| \le I_0F_m$ reaches J_cd when $I_0 = I_{th}$, and is obtained by

$$I_{th} = J_cd\,/F_m = J_cd/k, \tag{A.4}$$

where the (theoretical) coil coefficient is obtained by $k = F_m$.

When $I_0 > I_{th}$, the magnetic field penetrates below the superconducting film, and the nonlinear response of K_θ yields the generation of the harmonic voltages in the coil.

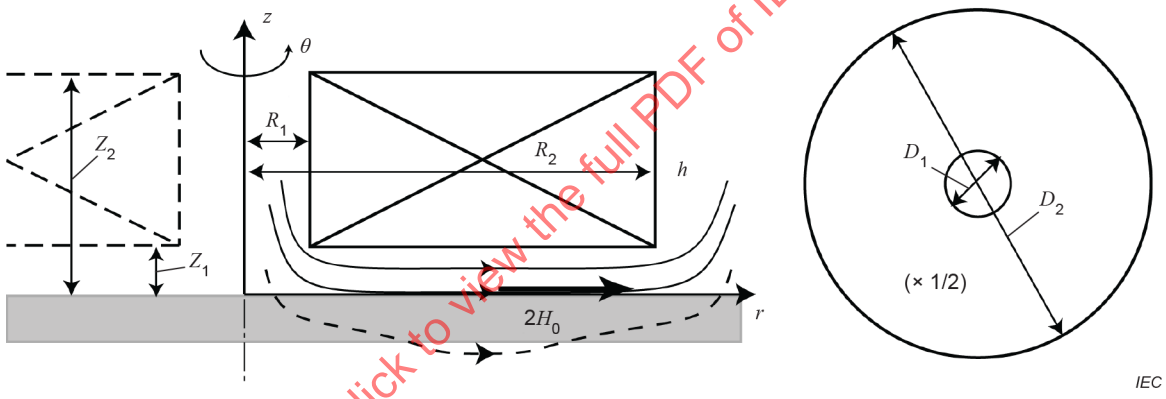

Figure A.1 – Illustration of the sample coil and the magnetic field during measurement

A.4 Calculation of the induced electric fields

Here, we approximate the average E induced in the superconducting film at the full penetration threshold, $I_0 = I_{th}$, using the Bean model [14]. This approximation assumes a semi-infinite superconductor below the xy-plane ($z \le 0$), and the film is regarded as part of this superconductor ($-d \le z \le 0$). When a sinusoidal magnetic field $H_{x0} = 2H_0\cos\omega t$ ($2H_0 = J_cd$) is applied parallel to the x-direction at the surface of the superconductor, the induced E has only the y-component $E_y(z)$, and $E_y(z \le -d)$ is zero because the magnetic fluxes just reach the lower surface of the film ($z = -d$). The $E_y(z)$ is calculated by integrating $-\mu_0(dH_x/dt)$ from $z = -d$ to z, yielding $E_y(z) = -\mu_0\omega dH_0\sin\omega t(1 - \cos\omega t + 2z/d)$. The time-dependent surface electric field, $|E_y(z = 0)|$, peaks at $\omega t = 2\pi/3$, and then, $\max|E_y(0)| = (3\sqrt{3}/4)\,\mu_0\omega dH_0$. Because $\max|E_y(z)|$ peaks at $z = 0$ (the upper surface of the film) and is zero at $z = -d$ (the lower surface of the film), the volume average of $\max|E_y(z)|$ is estimated to be half of $\max|E_y(0)|$,

$$E_{\text{avg-}U_3} \approx \left(3\sqrt{3}\pi/4\right)\mu_0 fdH_0 \approx 2{,}04\mu_0 fd^2J_c = 2{,}04\mu_0 kfdI_{th}\,. \tag{A.5}$$

For typical parameters of the measurement, f = 1 kHz, d = 250 nm, and J_c = 10^{10} A/m^2, the calculated E is about 2 μV/m.

A.5 Theoretical coil coefficient k and experimental coil coefficient k'

Here, the basic concept concerning the theoretical coil coefficient $k = J_c d/I_{th}$ and the experimental coefficient k' for the case of the U_3 inductive method is explained. When the coil current I_0 equals the threshold current I_{th}, the highest magnetic field below the coil $2H_{0,max} = J_c d$, and the magnetic field just fully penetrates the film. Since $2H_{0,max}$ can be theoretically calculated, we can calculate the theoretical coil coefficient $k = J_c d/I_{th}$. However, the above "true I_{th}" corresponds to the coil current at which infinitesimal U_3 is generated in the coil. Because it is impossible to detect $U_3 \approx 0$ to obtain a "true I_{th}", we need an alternative approach to obtain an "experimental I_{th}" and corresponding experimental coil coefficient k'.

A.6 Scaling of the U_3–I_0 curves and the constant-inductance criterion to determine I_{th}

For convenience, the (experimental) threshold current I_{th} has been often determined by a constant-voltage criterion, e.g. $U_3/\sqrt{2}$ = 50 μV. However, the use of a constant-voltage criterion is problematic. Theoretical analyses on the relationship between I_0 and U_3 showed that there is clear scaling behaviour $U_3/I_{th} = \omega G(I_0/I_{th})$, where G is a scaling function that is determined only by the specifications of the sample coil [11] [17]. This equation implies that the U_3 vs. I_0 curves with various I_{th} values must collapse to one curve if they are normalized with I_{th}. The inset of Figure A.2 a) clearly shows this scaling behaviour. As the third-harmonic resistance $U_3/I_0 = \omega G(I_0/I_{th})/(I_0/I_{th})$, the U_3/I_0 itself is already normalized (Figure A.2 b)), and it scales with the scaled current I_0/I_{th} (inset of Figure A.2 b)). Because the third-harmonic voltage U_3 is proportional to I_{th}, the determination of I_{th} by a constant-voltage criterion inherently causes a systematic error; namely, the J_c of a sample with $J_c d$ larger (smaller) than the standard sample is underestimated (overestimated) [16]. From the scaling behaviour observed in the third-harmonic resistance U_3/I_0 (Figure A.2 b)), it is demonstrated that the I_{th} should be determined by a constant-resistance criterion, such as U_3/I_0 = 2 mΩ. Furthermore, as the U_3 values are proportional to the measuring frequency, a constant-inductance criterion, such as U_3/fI_0 = 2 μΩ·s, should be used if the U_3 measurements are performed with multiple frequencies [16] [32]. It is also to be noted that such scaling behaviour forms the basis of the $J_c d$ measurement, the procedure for which is described in 6.2 to 6.4 using a standard sample (calibration wafer).

Because a supercurrent flowing in a superconductor is a function of electric field, it is recommended to determine J_c with a constant electric-field criterion using a multi-frequency approach through procedures described in 6.2 and 6.3. An example of the multi-frequency measurement is shown in Figure A.3 with $U_3/fI_0 = 2\pi L_c$ = 2 μΩ·s.